Alma Mater Studiorum – Università di Bologna

DOTTORATO DI RICERCA IN

SCIENZE CHIMICHE

Ciclo XXV

Settore Concorsuale di afferenza: 03-A2

Settore Scientifico disciplinare: CHIM-02

NANOTECHNOLOGY CONTROL OF SELF ORGANIZED BIOMOLECULES AND BIOMATERIALS FOR MEDICAL RESEARCH

Presentata da: Giulia Foschi

Coordinatore Dottorato

Prof.ssa Adriana Bigi

Relatore

Prof. Fabio Biscarini

Esame finale anno 2013

Dedico questo mio lavoro a tutta la mia famiglia e
al mio nonno che, anche se non c'è più,
mi è sempre vicino in ogni momento

TABLE OF CONTENTS

Key Words

Soft-lithograpy

Atomic Force Microscopy

Aggregation in confinement

Biofunctional scaffold

Regenerative medicine

Abbreviation & Acronyms

Aβ	Amyloid β
ACyD	Amphiphilic Cyclodextrin
AD	Alzheimer's Disease
AFM	Atomic Force Microscopy
AMID	Active Multifunctional Implantable organic Device
FDA	Food and Drug Administration
I-ONE	Implantable Organic Nano-Electronics
iPS cells	Induced Pluripotent Stem cells
MIMICs	MicroMolding in Capillaries
NPCs	Neural stem/Precursor cells
OFET	Organic Field Effect Transistor
PBS	Phosphate Buffer Solution
PDMS	Polydimethylsiloxane
PLGA	Poly(lactide-co-glycolic)acid
REM	Replica Molding
RMS	Root Mean Square
SCI	Spinal Cord Injury
SEM	Scanning Electron Microscopy
Tg	Glass Transition temperature

ABSTRACT

Nanotechnology entails the manufacturing and manipulation of matter at length scales ranging from single atoms to micron-sized objects. The ability to address properties on the biologically-relevant nanometer scale has made nanotechnology attractive for Nanomedicine. This is perceived as a great opportunity in healthcare especially in diagnostics, therapeutics and more in general to develop personalized medicine. Nanomedicine has the potential to enable early detection and prevention, and to improve diagnosis, mass screening, treatment and follow-up of many diseases. From the biological standpoint, nanomaterials match the typical size of naturally occurring functional units or components of living organisms and, for this reason, enable more effective interaction with biological systems. Nanomaterials have the potential to influence the functionality and cell fate in the regeneration of organs and tissues. To this aim, nanotechnology provides an arsenal of techniques for intervening, fabricate, and modulate the environment where cells live and function.

Unconventional micro- and nano-fabrication techniques allow patterning biomolecules and biocompatible materials down to the level of a few nanometer feature size. Patterning is not simply a deterministic placement of a material; in a more extended acception it allows a controlled fabrication of structures and gradients of different nature. Gradients are emerging as one of the key factors guiding cell adhesion, proliferation, migration and even differentiation in the case of stem cells.

The main goal of this thesis has been to devise a nanotechnology-based strategy and tools to spatially and temporally control biologically-relevant phenomena *in-vitro* which are important in some fields of medical research. In the following chapters the different techniques and applications are described. Chapter 1 makes a brief introduction on nanotechnologies, nanofabrication techniques and nanobiotechnology. In Chapter 2 an overview of the main fabrication and characterization techniques that I used in this work is given. Chapter 3 describes the study of β-Amyloid 1-40 peptide aggregation at solid-liquid interface in a confined environment artificially created by means of unconventional fabrication techniques, and aimed to mimick the effect of the cell crowding. This system is of interest in the etiology of Alzheimer's disease. In Chapter 4 the multiscale patterning of amphiphilic cyclodextrin bearing different cues for cell adhesion and growth has been achieved. In Chapter 5 I described the fabrication,

characterization and functionalization of a biodegradable scaffold that will be integrated with active electronic materials such as organic semiconductors and conductive electrodes, to yield an active multifunctional implantable organic device targeted to the stimulation, monitoring and regeneration of the Spinal Cord Injury. In Chapter 6 conclusions are given.

CHAPTER 1

Introduction

This chapter is dedicated to a brief introduction on the state of art of nanotechnologies, nanofabrication techniques and nanobiotechnology, with a particular focus on the thematic related to nanotechnology based on nanomaterials as interfaces with biological molecules or structures.

NANOTECHNOLOGY

Nanotechnologies underwent an incredible progress during the last decades, due to the huge development of fabrication and manipulation of nanometer-size objects. The driving force behind nanotechnology, other than miniaturization, is the recognition that nanostructured material have chemical and physical properties extremely different from those of bulk materials, and tunable by size. The properties that we associate with bulk materials are average properties, such as the density and the elastic modulus in mechanics, the resistivity and the magnetization in electricity and magnetism, and the dielectric permittivity in optics. Nanomaterials exhibit new phenomena associated with quantization effects and often the role of surfaces and interfaces is dominant. Quantization effects arise at the nanometer scale because the overall dimensions of objects are comparable to the characteristic wavelength of fundamental excitations in materials. These excitations carry the quanta of energy through materials and thus determine the dynamics of their propagation and transformation from one form to another. When the size of structures is comparable to the quanta themselves, the effect of the excitations moving through and interacting with material structures, is no more negligible, with the effect of bringing into play quantum mechanical selection rules not apparent at larger dimensions.

The term "nanotechnology" can be dated back to the 1959, when the physicist Richard Feynman presented his visionary and prophetic talk entitled "There's Plenty of Room at the Bottom" at the annual conference of the American Physical Society. He speculated on the potential applications of nano-sized materials. However, the birth of nanotechnology as a true technology begins with the invention of the Scanning Tunneling Microscope (STM) by Binnig and Rohrer in 1981[1]. STM made possible observing and manipulating, at the same time, materials down to single atom level[2].

NANOFABRICATION

Traditionally, materials can be fabricated following two different approaches: "top-down" and "bottom-up" (Figure 1.1).

In the "top-down" process a macroscopic object is progressively cut, carved, etched and shaped in order to obtain a smaller functional architecture. This is a subtractive approach. This methodology is characteristic of the conventional photolithographic techniques, which have been

used in microelectronics since many years to produce microchips and hardware components. However the resolution of photolithography, being an optical fabrication technique, is limited by the wavelength of the light. Features smaller than few microns are not achievable with this technique in UV-VIS. To overcome it, "top-down" techniques have been developed in the last decade, still based on light as X-ray Lithography (XRL)[3] and Deep X-ray lithography (DXRL)[4], or on De Broglie wavelength of the electrons as Electron Beam Lithography (EBL)[5]. All this technique allow one to achieve a very high resolution but require very expensive equipment and are not applicable to a large range of materials.

The "bottom-up" approach starts directly from the molecules or nano-scale building blocks, whose capability to self-assembly into regular structures under specific conditions is designed. The driving forces of this self-organization are specific and non-specific supramolecular and intermolecular interactions[6]. The forces responsible for the spatial organization vary from weak interactions (electrostatic and magnetic forces, hydrogen bonding) to strong interactions (covalent and ionic bonding). Non-covalent bonds are critical in maintaining the 3D structure of large molecules, such as proteins, nucleic acids and artificial supramolecular structures, and are involved in many biological processes in which large molecules bind specifically but transiently to one another. There are four commonly mentioned types of non-covalent interactions: hydrogen bonds, ionic bonds, van der Waals forces, and hydrophobic interactions. Examples of "bottom-up" techniques exploiting molecular self-organization are: Dip-pen Lithography (DPL)[7], Local Oxidation Nanolithography (LON)[8], Nanoimprint Lithography (NIL)[9] and Soft-lithography[10]. Thanks to their versatility and rapid prototyping, and possibility to be used with a variety of materials, "bottom-up" techniques have gained in importance in these decades for applications in diverse scientific fields, ranging from electronics, optoelectronics to biotechnology and medicine.

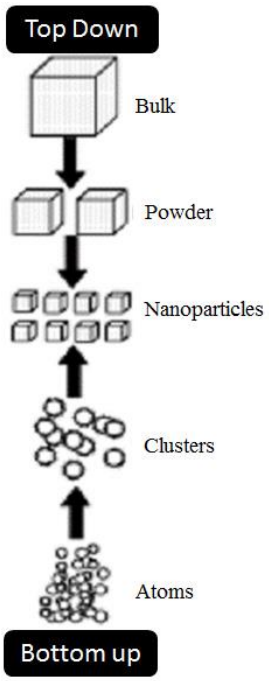

Figure 1.1 Schematic representation of the two fabrication approaches.

NANOBIOTECHNOLOGY

Nanotechnology is a novel scientific approach that involves materials and equipments capable of manipulating physical as well as chemical properties of a substance at the nanometer scale. On the other hand, biotechnology uses the knowledge and techniques of biology to manipulate molecular, genetic and cellular processes to develop products and services and is used in diverse fields from medicine to agriculture. Nanobiotechnology is considered to be the unique fusion of biotechnology and nanotechnology by which classical micro-technology can be merged to a molecular biological approach in real. Through this methodology, molecular grade machines can be made by mimicking or incorporating biological systems, or by building tiny tools to study or modulate diverse properties of a biological system on molecular basis. Nanobiotechnology may, therefore, ease many avenues of life sciences by integrating cutting-edge applications of information technology and nanotechnology into contemporary biological issues. This technology has potential to remove obvious boundaries between biology, physics and chemistry to some extent, and shape up our current ideas and understanding. For this reason, many new challenges and directions may also arise in education, research and diagnostics in parallel by the extensive use of nanobiotechnology with the passage of time.

In the last 15-20 years, the biological and medical research communities have exploited the unique properties of nanomaterials for various applications, and, because of the positive demonstrations, new avenues and promises have been created for nanotechnology research. Terms such biomedical nanotechnology, nanobiotechnology and nanomedicine are used to describe this convergence field. There seems to be a natural fit between nanotechnology and biology. With nanotechnology, a large set of materials with distinct properties (optical, electrical or magnetic) can be fabricated. Functionalities can be added to nanomaterials by interfacing them with biological molecules or structures. Furthermore, the size of nanomaterials is similar to that of most biological molecules and structures; therefore, nanomaterials can be useful for both *in-vivo* and *in-vitro* biomedical research and applications. Nanotechnology based on nanomaterials has opened a new era of technology which impacts on all sectors of human life.

Bibliography

[1] G. Binning, H. Rohrer, C. Gerber, E. Weibel, *Phys. Rev. Lett.* **1982**, *49*, 57-61.

[2] H. C. Manoharan, C. P. Lutz, D. M. Eigler, *Nature* **2000**, *403*, 512-515.

[3] H. I. Smith, M. L. Schattenburg, S. D. Hector, J. Ferrera, E. E. Moon, I. Y. Yang, M. Burkhardt, *Microelectron. Eng.* **1996**, *32*, 143-158.

[4] W. Ehrfeld, H. Lehr, *Radiat. Phys. Chem.* **1995**, *45*, 349-365.

[5] J. A. Liddle, G. M. Gallatin, L. E. Ocola, in *Three-Dimensional Nanoengineered Assemblies, Vol. 739* (Eds.: T. M. Orlando, L. Merhari, D. P. Taylor, K. Ikuta), **2003**, pp. 19-30.

[6] a) A. M. Higgins, R. A. L. Jones, *Nature* **2000**, *404*, 476-478; b) S. Herminghaus, K. Jacobs, K. Mecke, J. Bischof, A. Fery, M. Ibn-Elhaj, S. Schlagowski, *Science* **1998**, *282*, 916-919.

[7] W. Shim, A. B. Braunschweig, X. Liao, J. Chai, J. K. Lim, G. Zheng, C. A. Mirkin, *Nature* **2011**, *469*, 516-521.

[8] R. Garcia, R. V. Martinez, J. Martinez, *Chem. Soc. Rev.* **2006**, *35*, 29-38.

[9] S. Y. Chou, P. R. Krauss, P. J. Renstrom, *J. Vac. Sci. Technol. B* **1996**, *14*, 4129-4133.

[10] Y. N. Xia, G. M. Whitesides, *Angew. Chem., Int. Ed.* **1998**, *37*, 551-575.

CHAPTER 2

Experimental Methods

In this chapter, an overview of the main techniques used for fabrication and patterning is given. The characterization techniques that I used in this work are described.

Fabrication Techniques

2.1 Photolithography

Photolithography is the work-horse technology for microfabrication both in industrial production and in research laboratories. Its purpose is to transfer a drawing or a pattern from a mask to the surface of a planar substrate, for instance a silicon wafer. The pattern is created by exposure of a photoresistive film to light, either through a proximity mask or a projected image.

In planar technology, the steps following the exposure of the photoresist involve etching, deposition, and lift-off of the sacrificial layer. The steps involved in this process are: wafer cleaning, photoresist application, soft baking, mask alignment, exposure, development and hard-baking (Figure 2.1).

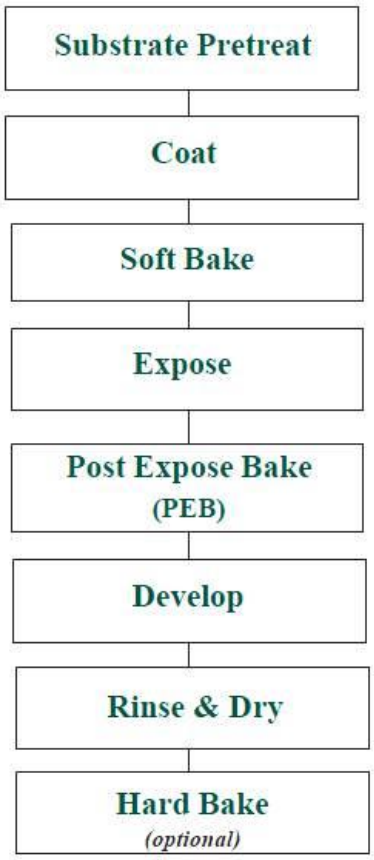

Figure 2.1 Steps involved in the photolithographic process (from www.microchem.com).

WAFER CLEANING AND PHOTORESIST APPLICATION

In the first step, a silicon wafer is chemically cleaned to remove particulate material on the surface as well as any trace of organic, ionic, and metallic impurities. To obtain maximum process reliability, substrates should be clean and dry prior to applying the photoresist. Start with a solvent cleaning, or a rinse with dilute acid, followed by a de-ionized water rinse. Where applicable, substrates should be subjected to a piranha etch/clean (H_2SO_4 and H_2O_2 1:1). To dehydrate the surface, bake at 200°C for 5 minutes on a hotplate, is required.

After cleaning, a photoresist is applied to the surface of the wafer by Spin Coating. In order to create a thin uniform layer of resist on the wafer surface, the parameters of the spin coater, such as rounds per minute, acceleration and time, must be accurately set.

There are two types of photoresist: positive and negative. For positive resists, the resist is exposed with UV light wherever the underlying material is to be removed. In this case, the UV exposure changes the chemical structure of the resist so that it becomes more soluble in the developer. The exposed resist is then washed away by the developer solution, leaving windows of the bare underlying material. In other words, "whatever shows, goes", with the mask containing the exact copy of the desired pattern. Negative resists behave in just the opposite manner. Exposure to the UV light causes the negative resist to become polymerized and more difficult to dissolve. Therefore, the negative resist remains on the surface wherever it is exposed, and the developer solution removes only the unexposed portions. Masks used for negative photoresists, therefore, contain the inverse of the pattern to be transferred. Figure 2.2 shows the different patterns generated with a negative and positive resist.

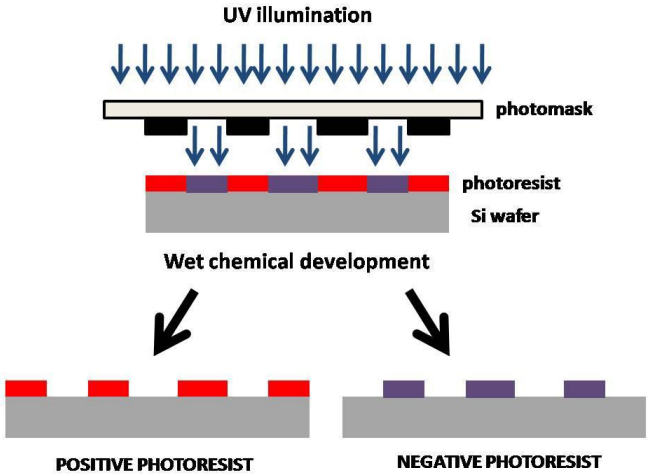

Figure 2.2 Different pattern obtained starting from a positive or negative photoresist layer.

SOFT BAKING

This is a critical step during which almost all of the solvent is removed from the photoresist coating according to a precise heating protocol. Soft baking plays a very critical role in photo-imaging because the photoresist coating becomes photosensitive only after this part of the process. Over soft baking will degrade the photosensitivity of resists by either reducing the developer solubility or actually destroying a portion of the sensitizer. Under soft baking will prevent light from reaching the sensitizer. Positive resists are incompletely exposed if considerable solvent remains in the coating. This under soft baked positive resists is then readily attacked by the developer in both exposed and unexposed areas, causing less etching resistance.

MASK ALIGNMENT AND EXPOSURE

One of the most important steps in the photolithography process is mask alignment. A mask is a plate with a patterned emulsion of metal film on one side. It is aligned with the wafer, so that the pattern can be transferred onto the wafer surface. Then the photoresist is exposed through the pattern on the mask with a high intensity ultraviolet light. There are three primary exposure methods: contact, proximity and projection. In our lab we used only the first method. In contact printing, the resist-coated silicon wafer is brought into physical contact with the mask. The wafer is held on a vacuum chuck, and the whole assembly rises until the wafer and mask contact each other. The photoresist is exposed to UV light while the wafer is in contact position with the mask. Because of the contact between the resist and mask, very high resolution can be achieved (e.g. 1-micron features in 0.5 microns of positive resist). One drawback is that debris trapped between the resist and the mask can damage the mask and cause defects in the pattern.

DEVELOPMENT AND HARDBAKING

One of the last steps in the photolithographic process is development. Its effectiveness strongly depends on the initial exposure conditions (time and beam energy) and photoresist characteristics. At low exposure energies, the negative resist remains completely soluble in the developer solution. As the exposure is increased above threshold energy, most of the resist film remains after development. At exposures two or three times the threshold energy, very little of the resist

film is dissolved. For positive resists, the resist solubility in its developer is finite even at zero exposure energy. The solubility gradually increases until, at some threshold, it becomes completely soluble. These curves are affected by all the resist processing variables: initial resist thickness, soft bake conditions, developer chemistry, developing time and others.
Hard baking is the final step in the photolithographic process. This step is necessary in order to harden the photoresist and improve its adhesion to the wafer surface.

2.2 Soft-lithography

Although photolithography is the dominant technology for microfabrication, even for large features, it is not always the best option for all applications because of several drawbacks: it is an expensive technology when features size is pushed below micron scale; it is poorly suited for patterning non planar surfaces; it provides almost no control over the chemistry of the surface and hence is not very flexible in generating patterns of specific chemical functionalities on surfaces; it can generate only two dimensional microstructures and it is directly applicable only to a limited set of photosensitive materials. During the nineties, G. M. Whitesides and co-workers investigated and developed a set of non-photolithographic methods that was termed soft-lithography[1], as a new approach for rapid prototyping, low cost and versatile micro-nanofabrication methods. The breakthrough idea was to exploit the interplay between surface and capillary forces acting between an elastomeric stamp and a substrate and the self-organization of the molecules on the substrate that is mainly governed by non-covalent interactions, to create patterns of a molecular or polymeric material.

Nowadays soft-lithography allows patterning of a variety of molecules and materials including adhesion proteins[2], nucleic acid[3], ceramic[4] and polymeric material[5]. Soft-lithography encompasses several techniques sharing as a key element an elastomeric stamp or mold with patterned relief structures on its surface. The principal techniques are Microcontact Printing (μcP)[6], Replica Molding (REM)[7], MicroTransfer Molding (μTM)[8], MicroMolding in Capillaries (MIMICs)[9] and Solvent Assisted Microcontact Molding (SAMIM)[10]. The most used elastomeric materials is polydimethylsiloxane (PDMS, Figure 2.3) and in its most widely commercialized version (Sylgard 186, Dow Chemicals) is supplied as two components, a base and a curing agent[11].

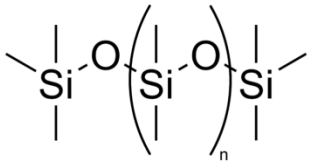

Figure 2.3 Siloxane backbone of PDMS.

Silicon hydride groups present in the curing agent react with vinyl groups present in the base and form a cross-linked elastomeric solid. To produce a replica, it is necessary to mix the two parts together (typically 10:1 v/v base:curing agent), pour the liquid pre-polymer over the master and cure it. The liquid PDMS pre-polymer conforms to the shape of the master and replicates its features with high fidelity. In particular PDMS can percolate even into very small recess enabling the reproduction of nanometer topographical details. Hence the resolution limit of soft-lithography is set only by the materials properties (e.g. Van der Waals interactions, solubility, diffusivity) rather than by sample transparency and optical diffraction as for conventional Photolithography. The low surface free energy and elasticity of PDMS allow it to release from masters without damaging the master or itself. In fact, PDMS is even more than a structural material, its chemical and physical properties make possible fabrication of devices with useful functionality (Table 2.1)[11].

Table 2.1 Principal physical and chemical properties of PDMS.

Property	**Characteristic**
Optical	Transparent; UV cutoff, 240 nm
Electrical	Insulating; breakdown voltage, $2x10^7$ V/m
Mechanical	Elastomeric; tunable Young's modulus, typical value of ~ 750kPa
Thermal	Insulating; thermal conductivity, 0.2 W/(m*K); coefficient of thermal expansion, 310 μm/(m*°C)
Interfacial	Low surface free energy ~20 erg/cm^2
Permeability	Impermeable to liquid water; permeable to gases and nonpolar organic solvents
Reactivity	Inert; can be oxidized by exposure to a plasma; $Bu_4N^+F^-$ ((TBA)F)
Toxicity	nontoxic

One advantage of PDMS is that it can seal to itself, or to other surfaces, reversibly or irreversibly and without distortion of the channels. A reversible seal is provided by simple Van der Waals contact between PDMS molded against a smooth surfaces, while to form an irreversible seal the PDMS has to be exposed to air or oxygen plasma[12]. This treatment generates silanol groups (Si-OH) on the surface of the PDMS by the oxidation of methyl groups[13]. Surface oxidized PDMS can seal to itself, glass, silicon, polystyrene, polyethylene or silicon nitride, provided that these surfaces have also been exposed to the plasma. Quake and co-workers have developed an alternative method for irreversibly sealing that involves adding an excess of the base to one slab of PDMS and the curing agent to another slab[14]. When these layers were brought into conformal contact and again cured, the seal that formed was indistinguishable in physical properties from the bulk PDMS.

In Figure 2.4 the processing steps of soft-lithographic fabrication are depicted.

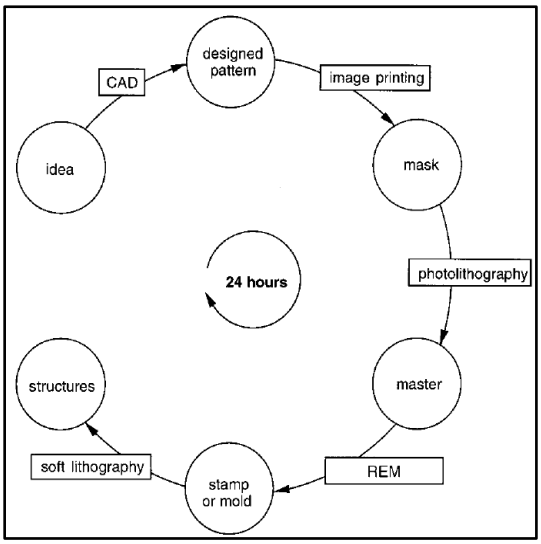

Figure 2.4 Rapid prototyping procedure for soft-lithography (adapted from G. M. Whitesides et al.[15]).

Starting from the original idea, the pattern is transferred to a CAD file and printed on a transparent sheet of polymer with a commercial image setter. This patterned sheet is used as a mask to prepare the master in a thin film of photoresist; a negative replica of this master with an elastomeric material becomes the stamp or mold for soft-lithography. One can start also from a commercial mask (usually of chromium/quartz or polyester). The overall cycle from design to stamp takes less than 24 hours to be completed. However, once one has the master, tens of stamp

can be obtained by Replica Molding (REM) before the master deteriorates, allowing a great time-saving. This is another advantage of soft-lithography over conventional photolithography.

2.3 Replica Molding

REM yields a negative duplicate of the topographic information present in a master, even if three dimensional. In REM, an appropriate elastomer such as PDMS, enables replicating highly complex master structures with nanometer features in a simple, reliable and inexpensive way. The general replication procedure is reported in Figure 2.5.

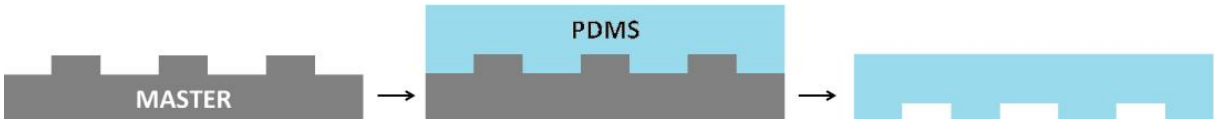

Figure 2.5 Replica molding steps of a rigid master with PDMS.

The molds are prepared by casting against rigid master a mixture of PDMS and curing agent, typically in a ratio 10:1. The PDMS-master is put in an oven at 90°C for 2 hours to complete the curing process. Then the mold is peeled off and is ready to be used as stamp. This process can be replicated tens of times on the same master without introducing any defects. This is a practical protocol for manufacturing multiple copies of indistinguishable nanostructures from a single master.

2.4 MicroMolding in Capillaries

MicroMolding in Capillaries (MIMICs) is a simple and versatile soft-lithographic method that gives rise to complex microstructures on both planar and curved surfaces. It was introduced by G. M. Whitesides and co-workers in 1995[16]. MIMICs, whose scheme is reported in the Figure 2.6, can be considered as a prototype of micro- and nano-fluidics, and it can be used to pattern many soluble materials.

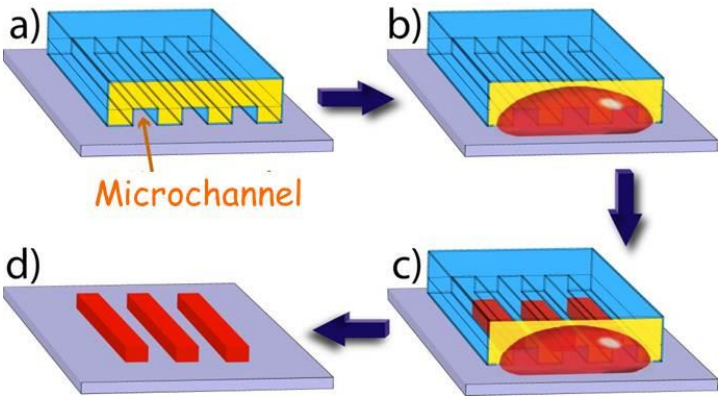

Figure 2.6 Schematic representation on the MIMICs process.

MIMICs is based on the spontaneous filling of capillaries formed between two surfaces in conformal contact, at least one of which has a recessed relief structure, by a fluid. In particular, in a master for MIMICs, the motif consists of protruding lines that become grooves in the PDMS replica. When the stamp is placed in contact with the surface under study, the nature of PDMS allows conformal contact between the mold and the surface, and a network of channels forms (Figure 2.6a). When a solution containing the relevant material is placed at the open end of the stamp (Figure 2.6b), capillary pressure drives the solution inside the channels (Figure 2.6c) and the solute starts to precipitate when super-saturation is achieved following solvent evaporation. No residual layer is deposited in areas where adhesive conformal contact between mold and substrate is established. After the complete evaporation of the solvent the PDMS stamp is gently removed leaving the micro- and nano-structures on the surface (Figure 2.6d). The size of the channels, together with the concentration of the solution and the self-organizing properties of the solute, determine the length scale of the pattern that can be controlled with this process. Feature sizes ranging from millimeters to tens of nanometers have been demonstrated. In the following, the influence of surface tension and fluid viscosity will be discussed.

Despite of its apparent simplicity, MIMICs is a more complicated process, and some rationale is needed in order to control the spatial distribution of the deposited solute. MIMICs is a thermodynamically driven process, the liquid fills the capillaries to minimize the free energy of the solid-vapor and solid-liquid interfaces. The problem is to fabricate an array of channels having surface tension that promote capillary filling[9].

A zero-th order model of MIMICs is described in the following, referring to Figure 2.7. First, we assume that $\gamma_{SV} = \gamma_{S'V}$. The liquid, whose liquid-vapor tension γ_{LV}, fills the channel driven by Laplace pressure[17]:

$$\Delta P = 2\gamma_{LV} \cos\theta / r.$$

The contact angle θ is defined by Young's equation:

$$\cos\theta = (\gamma_{SV} - \gamma_{SL})/\gamma.$$

The surface tensions γ_{SV} and γ_{SL} depend on the substrate and the channel walls, and r is the effective diameter of the channel.

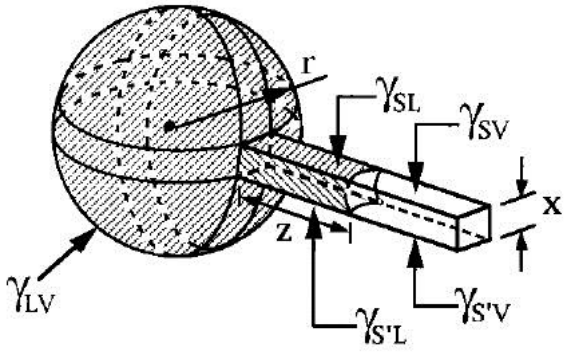

Figure 2.7 A model for MIMICs. A fluid is assumed to move from a spherical drop (radius *r*) into a square channel (width *x*) with three identical surfaces (PDMS) and one different (the substrate). The terms γ_{SV}, γ_{SL}, and γ_{LV} corresponds to interfacial free energies of solid-vapor, solid-liquid and liquid-vapor interfaces (from G. M. Whitesides et al.[9])

The rate of the liquid flow[16] in the capillary is determined by the ratio of surface tension and viscosity of the liquid, the cross-sectional dimension of the capillary and the length of the channel by the follow equation[18]:

$$\frac{dz}{dt} = \frac{R\gamma_{LV}\cos\theta}{4\eta z} = \frac{R(\gamma_{SV} - \gamma_{SL})}{4\eta z}$$

where R is the hydrodynamic radius, the ratio between the volume of the liquid in the capillary section and the area of the solid and liquid interface, η the viscosity of the liquid, z the length of the column of liquid (Figure 2.7). Upon integration of the differential equation, one obtains the filling distance *vs* time:

$$z(t) = \sqrt{\frac{R(\gamma_{SV} - \gamma_{SL})t}{2\eta}}$$

The equations clearly show that the maximum rate is achieved when $\cos\theta \geq 1$, i.e. when the liquid wets the channel walls, and its surface tension is high. Viscosity opposes infilling. With all fluids, the rate of filling is inversely proportional to the length of capillary: filling velocity decreases as the capillary is infilled. This result assumes that the four walls delimiting the capillary have homogeneous interfacial free energies.

In MIMICs, the three surfaces of the PDMS channels have a different interfacial free energy γ_{SV} with respect to $\gamma_{S'V}$ of the substrate (Figure 2.7).

When γ_{SV} is lower than $\gamma_{S'V}$, an aqueous solution (high γ_{LV}) wets the substrate while does not wet the PDMS walls. The solute will be deposited mostly on the substrate. A fluid with low surface tension wets largely the PDMS walls, but not a high-surface tension substrate (e.g. glass). In either case, one of the two materials opposes the infilling, yielding an inhomogeneous advancing fluid front and hence inhomogeneous deposition (Figure 2.8). Fluids with an intermediate surface tension, for example methanol or ethanol, represent a most useful compromise for filling velocity and homogeneous front. Alternatively, with high surface tension fluids, such as water, addition of a surfactant or an organic solvent drive the infilling, else a treatment of the channel walls in order to increase their surface tension is necessary.

The shape of the imbibition front of liquid precursors has been studied in detail[19]. Depending on the surface energy of the channel wall γ_{SV}, different spreading regimes can be observed, as illustrated in the Figure 2.8.

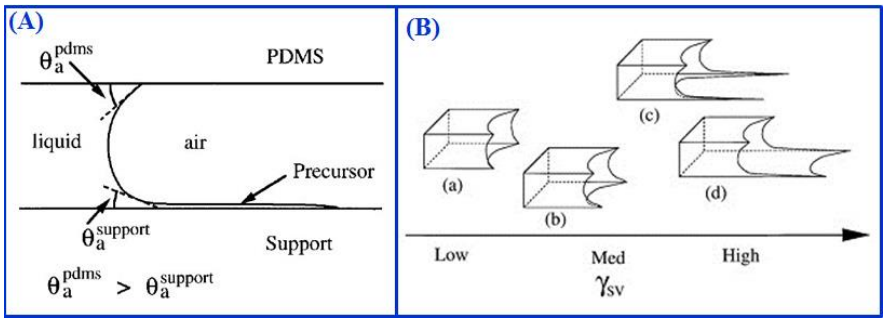

Figure 2.8 (A) Profile depicting the shape of the imbibition front showing different advancing contact angle of the liquid on PDMS and substrate. (B) Schematic representation of different spreading regimes

observed in MIMIC. Shapes of the penetration liquids in PDMS capillaries are formed inside (a) walls with low γ_{SV}, (b and c) walls with medium γ_{SV} and (d) walls with high γ_{SV}.

Liquids penetrating inside a channel with low surface energy walls, exhibit capillary fronts that advance as a whole. As the surface energy of the channel increases, solute structures advancing in front of the macroscopic body of liquid are observed, especially in the corners between mold and substrate. Some of these structures include slipping films and shoulders. Similar regimes have been observed with differences in the velocity of imbibition on surfaces of constant γ_{SV}[18].

Characterization Techniques

2.5 Optical Microscopy

Optical microscopy exploits UV-visible light to image objects. The simplicity of the technique and the minimal sample preparation required are significant advantages. The resolution limit is set by the Raleigh diffraction limit of the wavelength of the light, so objects spaced less than 0,2 micrometers are not distinguished.

The optical components of a modern microscope are shown in Figure 2.9. The optical path has to be very accurately set up and controlled. Despite of this, the basic operating principle of a microscope is quite simple. An objective lens with very short focal length (few millimeters) is used to form a highly magnified real image of the object. This magnification is carried out by means of two lenses: the objective lens which creates an image at infinity, and a second weak tube lens which forms a real image in its focal plane. The resulting image can be detected directly by the eye, imaged on a photographic plate brought onto the array detector of a digital camera.

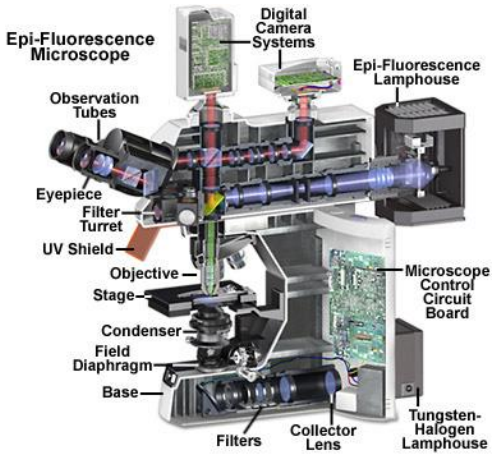

Figure 2.9 Components of a modern microscope configured for both transmitted and reflected light.

Techniques working with different illumination modes have been developed such as Bright field, Dark field, Phase contrast, Polarized light, Hoffman modulation contrast, Differential interference contrast, Fluorescence[20].

Bright field microscopy is the simplest, with the sample being illuminated by transmitted white light. It presents however some limitations such as it can only image dark or strongly refracting objects effectively. Dark field microscopy is an illumination technique used to enhance the contrast in unstained samples. To view a specimen in dark field, an opaque disc is placed underneath the condenser lens, so that only light that is scattered by objects on the slide can reach the eye. Instead of coming up through the specimen, the light is reflected by particles on the slide. This produces the classic appearance of a dark, almost black, background with bright objects on it. In this work, optical microphotographs have been recorded both in bright/dark field and in fluorescence mode with a Nikon 80i epifluorescence microscope (Tokio, Japan) equipped with a dark field system and crossed polars, using 5x, 10x, 20x and 50x short working distance objectives and a digital camera (Nikon High-speed Live Display Color Camera HeadDS-2Mv).

2.6 Scanning Electron Microscopy

WORKING PRINCIPLE

An electron microscope uses an electron beam for imaging objects, thus allowing a resolution orders of magnitude higher than optical microscopy. The development of the electron microscope

was based on theoretical work done by Louis de Broglie, who found that wavelength is inversely proportional to momentum. In 1926, Hans Busch discovered that magnetic fields could act as lenses by causing electron beams to converge to a focus. The first operational electron microscope was presented by Ernst Ruska and Max Knoll in 1932, and 6 years later Ruska had a first version on the market. In 1986 Ruska received a Nobel Prize in physics for his "fundamental work in electron optics and for the design of the first electron microscope". The original form of the electron microscope was a Transmission Electron Microscope (TEM), which uses high energy electrons to image the sample, while Scanning Electron Microscope (SEM) collects secondary electrons to get an image. Figure 2.10 shows the basic components of a SEM: (1) the electron column, (2) the specimen chamber, (3) the vacuum pumping system and (4) the electron control and imaging system.

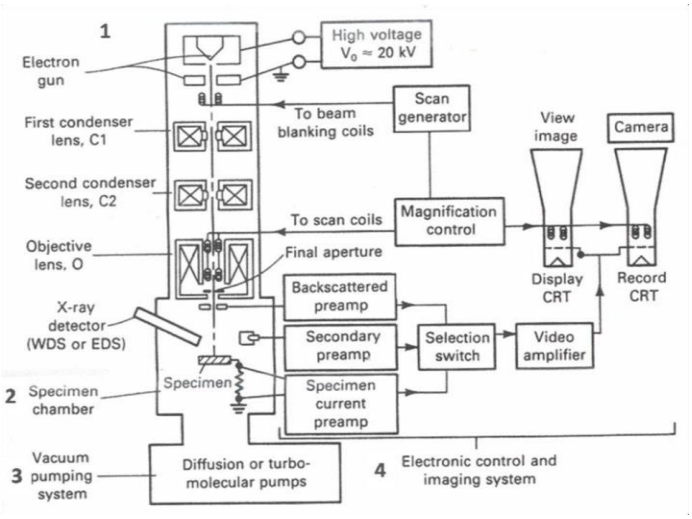

Figure 2.10 Schematic representation of SEM instrument.

In a typical configuration, an electron beam is thermionically emitted from an electron gun fitted with a tungsten filament cathode. Tungsten is normally used in thermionic electron guns because it has the highest melting point and lowest vapor pressure of all metals, thereby allowing it to be heated for electron emission, and because of its low cost. Other types of electron emitters include lanthanum hexaboride (LaB6) cathodes, which can be used in a standard tungsten filament SEM if the vacuum system is upgraded, and field emission guns (FEG), which may be of the cold-cathode type using tungsten single crystal emitters or the thermally-assisted Schottky type, using emitters of zirconium oxide. The field emission source provides higher resolution; high stability

and high current in a small spot size and generates high x-ray fluxes for chemical analysis at high resolution conditions. The electron beam, which typically has an energy ranging from 0.5 keV to 40 keV, is focused by one or two condenser lenses to a spot about 0.4 nm to 5 nm in diameter. The beam passes through pairs of scanning coils or pairs of deflector plates in the electron column, typically in the final lens, which deflect the beam in the x and y axes so that it scans in a raster fashion over a rectangular area of the sample surface.

When the electron beam strikes a sample, these electrons will scatter through the sample within a defined area called the interaction volume (Figure 2.11).

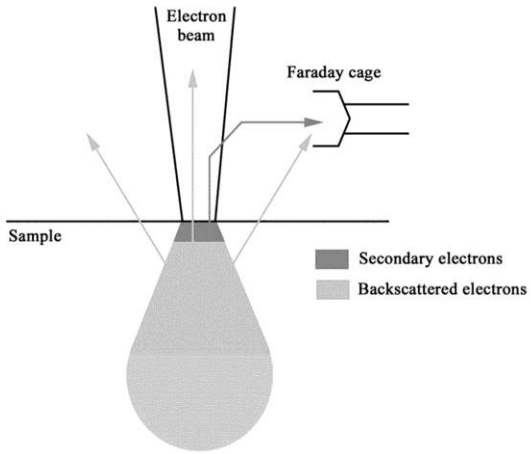

Figure 2.11 Scheme of the interaction between an accelerated electron beam and the sample.

During the electron beam-specimen interactions, many signals are produced, like transmitted electrons (TEM), secondary electrons (SEM), backscattered electrons (BSE) diffracted backscattered electrons (EBSD, that are used to determine crystal structures and orientations of minerals), photons (characteristic X-rays that are used for elemental analysis and continuum X-rays), visible light (cathode luminescence-CL), and heat. Secondary electrons are low energy electrons and when produced deeper within the interaction volume, will be absorbed by the sample. Only secondary electrons close to the surface will be able to escape the specimen. The weakly negative secondary electrons will be deflected by a positive pull exerted by the Faraday cage surrounding the secondary electron detector and therefore will contribute to the image formation. Backscattered electrons are also produced deep within the sample but have a much higher energy and because of this, are able to escape from deeper within the interaction volume. Because of their high energy, backscattered electrons will not be deflected by the Faraday cage

and therefore not contribute to the image formation. Only a few backscattered electrons will interfere with the signal for secondary electrons. The SEM used in this work is an Hitachi-S4000 FEG-SEM (Figure 2.12; max resolution: 1.5 nm; acceleration voltage: 0.5kV-30kV; magnification: 20X-200.000X; filament: cold-cathode field emission).

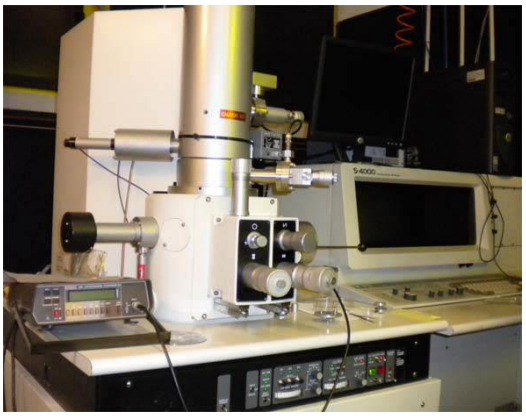

Figure 2.12 FEG-SEM Hitachi S-4000 (Institute for the Study of Nanostructured Materials, CNR Bologna)

SAMPLE COATING

For SEM imaging, samples must be electrically conductive and grounded to prevent electrostatic charge accumulation at the surface. Metal specimens require little preparation apart from a good conventional cleaning procedure. Instead, non-conductive specimens are usually coated with an ultrathin layer (few nm) of an electrically-conducting material (commonly gold, but also platinum, osmium, tungsten and graphite) deposited by low vacuum sputtering or high vacuum sublimation. Other than preventing charge accumulation, there are two reasons for coating: to increase signal and surface resolution, especially with samples containing low atomic number elements. The improvement in resolution arises mainly from the enhancing of the backscattering and secondary electron emission near the surface. Depending on the instrument, the resolution ranges between less than 1 nm and 20 nm. For SEM analysis, the sample is normally required to be completely dry, since the specimen chamber is at high vacuum; thus living cells and tissues usually require chemical fixation to preserve their structure.

2.7 Atomic Force Microscopy

WORKING PRINCIPLE

In 1982 G. Binning, H. Rohrer, C. Gerber and E. Weibel developed the scanning tunneling microscope (STM), opening a new era in surface science. The limitation of this technique is the possibility to scan only conductive surfaces. The invention of the Atomic Force Microscope (AFM), responding to van der Waals interactions rather than on the tunneling current, overcame this problem allowing the investigation of almost all the materials with physically relevant surface morphology. In more recent years other scanning probe techniques directly related to AFM have been introduced to probe also electric, magnetic and elastic properties.

AFM is a relatively compact instrument compared to electron microscope. It does not require vacuum to operate and can be placed on any stable workbench in a laboratory.

The key elements of an AFM are: 1) a local probe interacting with the surface; 2) a piezoelectric actuator which allows sample or probe (stand-alone configuration) motion; 3) an electronic system for the detection and the amplification of the signal resulting from the probe-sample interaction; 4) a feedback loop allowing to keep the probe-sample interaction stable by the definition of an appropriate set point; 5) a mechanical system to insulate the microscope from external mechanical or electrical coupling or noise. The basic operation mode is common to all the scanning probe techniques: a very sharp tip is attached to a cantilever spring that is scanned across a sample surface. When the tip is moved near the surface, different kind of interactions can take place, ranging from Van der Waals and dipole-dipole up to magnetic forces. These depend on the nature of the tip and sample, and the typical distance between them. The resulting cantilever spring displacement, acting as a small dynamometer, is recorded as relevant physical signal by an optical lever. A laser beam is focused on the cantilever with an incidence angle θ and reflected via one or more mirrors to a four segment Position Sensitive Detector (PSD), after an optical path L (Figure 2.13).

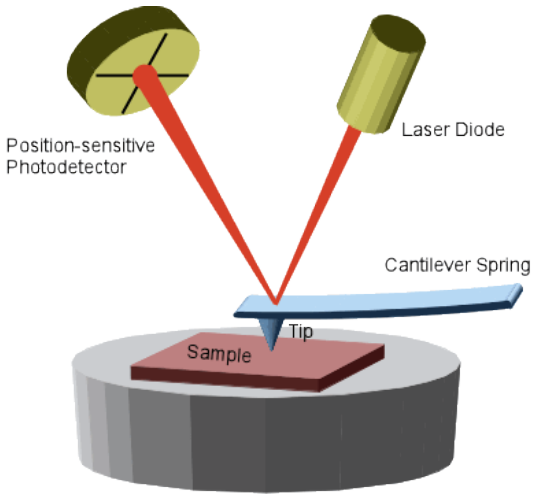

Figure 2.13 Schematic representation of AFM equipment.

Any small variation $\Delta\theta$ of the incidence angle will produce a Δz shift of the reflected spot in the photodiode, amplifying the angle variation as $\Delta z = L\Delta\theta$. This movement is detected by the PSD comparing the intensity of the signal from each segment, with a sub-Angström resolution. Two pairs of segments (upper and lower) give the values of vertical deflection of cantilever, known as topography or Z-signal. Another pair of segments (left and right ones) yields the so-called lateral force signal, related to the tilting of the cantilever due to torsional forces during scan.

The piezoelectric can contract or elongate under the application of an electric bias with the direction of the elongation that is perpendicular to that of the applied voltage, thus allowing the motion in the x-y-z space. The Z signal goes to the Feedback electronics, which controls the piezoelectric scanner and regulates the interaction strength moving the piezoelectric in order to minimize the difference between the measured value and the required one.

THE CANTILEVER

As already mentioned, the probe of an AFM is the crucial part of the instrument and is made of a sharp tip (whose curvature radius in the order of nanometers) attached to a cantilever type-spring (on the order of microns).

The side of the cantilever opposite to the tip is fixed to a millimeter sized chip, which can be easily handled. The cantilever responds according to Hook's law, allowing to translate small forces into detectable displacements:

$$F = -k\Delta z$$

the resonance frequency of the cantilever is:

$$W_o = \sqrt{\frac{k}{m}}$$

for a rectangular cantilever (diving board) the spring constant *k* is calculated from the equation:

$$k = \frac{Ewt^3}{4l^3}$$

where E is the Young's modulus of the cantilever and l, w and t its length, width and thickness respectively. For example, to obtain a resonance frequency W_0 in the range 10-100 KHz with a cantilever spring constant of ~0.1-1 N/m it is necessary a lever approximately 100 μm long and 1 μm thick. Such sizes are nowadays achievable by means of common micro-fabrication techniques.

To be effective the force sensor has to fulfill several requirements:

i) the spring constant *k* has to be small enough to detect small forces;

ii) the resonant frequency W_0 has to be high enough to minimize sensitivity to mechanical vibrations.

iii) the tip has to be sharp enough to achieve high lateral resolution (of the order of 10^{-10} m).

The tip curvature is the real radius of the tip in the approximation that it is spherical and determines the size of the details that the AFM will be able to resolve. The aspect ratio instead is a measure of the opening angle of the cone representing the full tip, and establishes how deep the tip will penetrate between two adjacent structures on the surface.

OPERATING MODES

Many forces are involved in the interaction between tip and surface. However the most relevant are van der Waals forces which arise from dipole-dipole attractive interactions and ion core repulsive interaction. For pairs of atoms these forces are described by the Lennard-Jones potential:

$$V(r) = c_1 \frac{1}{r^{12}} - c_2 \frac{1}{r_6}$$

where r is the distance from the surface, c_1 and c_2 are appropriate constants, the term to the sixth power of r represents the attractive van der Waals potential while the term r_{12} represents the strong repulsive potential when the tip is close to the surface.

The sum of van der Waals pair interactions is a good approximation to the interaction between tip and sample. The sum runs on all atoms of the tip and on the substrate, therefore is effectively an integral of the pair potential on the volumes of tip and substrate. This leads to smaller exponents in both the attractive and the repulsive terms, or equivalently makes the potential to be long ranged with respect to the L-J potential. The force between tip and sample is the negative derivative of such potential, and is schematically depicted in Figure 2.14.

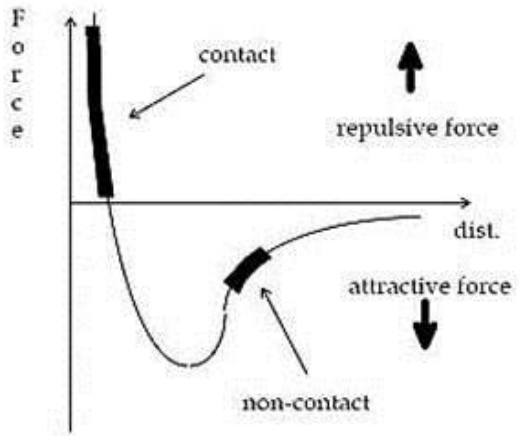

Figure 2.14 Typical force-curve for a tip surface interaction.

When the cantilever is far from the surface, the cantilever is in the attractive force regime and the potential varies slowly: the AFM operation mode is called “non-contact mode”. A stiff cantilever is forced to oscillate at a certain distance to the sample, without touching it. The forces between the tip and sample are quite low, of the order of pN (10^{-12} N). The detection scheme is based on measuring changes of the resonant frequency or of the oscillation amplitude of the cantilever.

On the contrary, if the cantilever works in the repulsive force regime, viz. very near to the surface, the operation mode is called “contact mode”. This mode enables a very high resolution but it enhances the probability to damage the cantilever. In constant force mode, the tip is constantly adjusted to maintain a constant deflection, and therefore constant distance from the surface. It is this adjustment that is displayed as topographic data. Because the tip is in hard

contact with the surface, the stiffness of the lever needs to be less that the effective spring constant holding atoms together, which is on the order of 1-10 nN/nm. Most contact mode levers have a spring constant of < 1N/m.

There is a third operation mode that is “tapping mode”, and that is the one used in this thesis.

In this mode the cantilever is excited externally with constant excitation amplitude at a constant frequency near its resonance frequency. While scanning the surface, a feedback loop controls the cantilever-sample distance in order to maintain the amplitude constant. Typical oscillation amplitudes are in the range of 10 to 100 nm, thus encountering a wide range of tip-sample interactions within each cycle, including both attractive as well as repulsive forces.

The feedback system detects also the oscillation shift (phase signal), which can provide information about the surface composition and viscoelastic properties.

In this thesis a Smena (NT-MDT, Zelenograd, Russia) scanning probe microscope (Figure 2.15) has been used. This microscope consists of standalone head, where the piezo scanner is positioned inside the head. The geometry of the piezo consists of three blocks of piezoelectric ceramic, they allow the movement of the tip in three orthogonal directions x, y, z. The sample is placed on a special sample holder, and the head is the only moving part. The microscope is equipped with a camera and often with a vibration insulator.

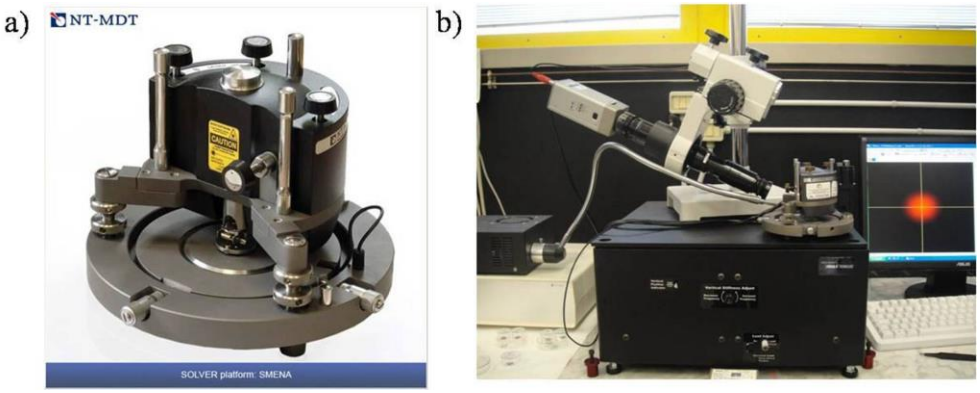

Figure 2.15 (a) NT-MDT^{TM} Smena Standalone head, (b) AFM equipment (Institute for the study of Nanostructured Materials, CNR-Bologna, Italy).

2.8 Wettability Measurements

In many applications the wettability of a surface or ability of liquids to wet surfaces can be a key factor in a product's performance or be a significant issue in a manufacturing process, for examples cleaning of glassware, lubrication, crop spraying, photographic processing, coating surfaces, etc.

Wetting refers to the study of how a liquid deposited on a solid (or liquid) substrate spreads out. When a drop is placed down on very clean glass, it spreads completely. By contrast, the same drop deposited on a sheet of plastic remains stuck in its place. The conclusion is that two regimes of wetting can be identified: total and partial wetting (Figure 2.16a), according to the difference between the surface tension, viz. the surface energy per unit area E_{sub} of the dry substrate and that of the wet substrate. The parameter distinguishing the two regimes is called spreading parameter S[17c]:

$$S = [E_{sub}]_{\text{dry}} - [E_{sub}]_{\text{wet}} = \gamma_{SV} - (\gamma_{SL} + \gamma)$$

where the three coefficients γ are the surface tensions at the solid-air, solid-liquid and liquid-air interfaces respectively. In total wetting the parameter S is positive and, as a result of the competition between molecular and capillary forces, the liquid spreads completely forming a continuous thin film with contact angle θ=0. In partial wetting, S is negative and the liquid does not spread forming at equilibrium a hemi-spherical cap resting on the substrate with a non-zero contact angle. Depending on the contact angle, the liquid is "mostly wetting" when $\theta \leq \pi/2$ whereas is "mostly non-wetting" when $\theta > \pi/2$ (Figure 2.16b)[17c].

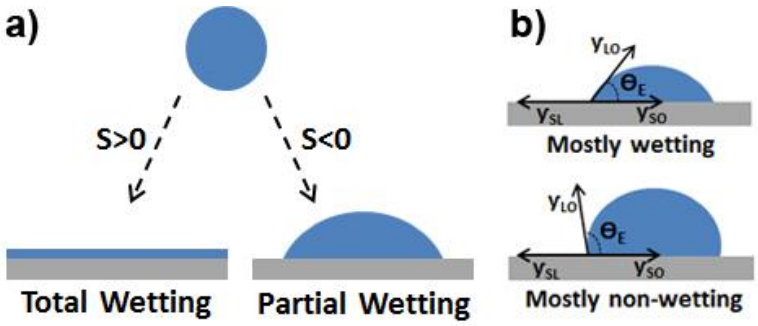

Figure 2.16 Schematic drawing of (a) the two wetting regimes, and (b) drops of "mostly wetting" and "mostly non-wetting" liquids on a solid substrate.

The contact angle is a measure of the ability of a liquid to spread on a surface. The method consists to measure the angle between the outline tangent of a drop deposited on a solid and the surface of this solid. The contact angle is also linked to the surface energy.

A contact angle measurement gives some different information:

• the affinity of a liquid to a solid surface. If water is used to measure the contact angle one can deduce the hydrophobic ($\theta > 90°$) or hydrophilic ($\theta < 90°$) character of the surface;

• if several reference liquids are used, the surface energy of the solid can be calculated, discriminating between polar and dispersive components.

• the measure of the hysteresis between advancing angle and recessing angle give informations on non-homogeneity of the surface (roughness, contamination, etc).

One approach commonly used to measure contact angles of solid substrates is the optical tensiometry (goniometry). Optical tensiometry involves the observation of a sessile drop of a liquid on the substrate. Analysis of the shape of a drop of test liquid placed on a solid is the basis for optical tensiometry. The basic elements of an optical tensiometer include a light source, sample stage, a siring to make the droplet, lens and image capture device (Figure 2.17). The contact angle instrument used all along this work is a contact angle meter DGD - DX model (DIGIDROP).

Contact angle can be accessed directly by measuring the angle formed between the solid and the tangent to the drop surface. With this technique it is possible to use a great variety of solid substrates provided they have a relatively flat portion for testing, and can fit on the stage of the instrument. Testing can be done using very small quantities of liquid.

The assignment of the tangent line that defines the contact angle is a factor which can limit the reproducibility of contact angle measurements. Conventional optical tensiometry relies on the consistency of the operator in the assignment of the tangent line. This can lead to significant error, especially subjective error between multiple users. In some case it is possible to analyze the drop by using computer analysis of the drop shape to generate consistent contact angle data.

In addition the amount of surface sampled for each measurement is limited and multiple measurements should be used to characterize a surface.

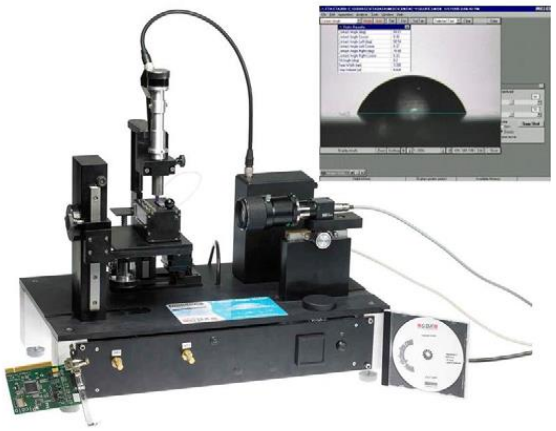

Figure 2.17 Photo of a contact angle instrument.

Bibliography

[1] Y. N. Xia, J. A. Rogers, K. E. Paul, G. M. Whitesides, *Chem. Rev.* **1999**, *99*, 1823-1848.

[2] N. Sgarbi, D. Pisignano, F. Di Benedetto, G. Gigli, R. Cingolani, R. Rinaldi, *Biomaterials* **2004**, *25*, 1349-1353.

[3] E. Bystrenova, M. Facchini, M. Cavallini, M. G. Cacace, F. Biscarini, *Angew Chem Int Ed Engl* **2006**, *45*, 4779-4782.

[4] C. R. Martin, I. A. Aksay, *Journal of Electroceramics* **2004**, *12*, 53-68.

[5] W. S. Beh, I. T. Kim, D. Qin, Y. N. Xia, G. M. Whitesides, *Adv. Mater.* **1999**, *11*, 1038-1041.

[6] A. Kumar, G. M. Whitesides, *Abstr. Pap. Am. Chem. Soc.* **1993**, *206*, 172-COLL.

[7] Y. N. Xia, E. Kim, X. M. Zhao, J. A. Rogers, M. Prentiss, G. M. Whitesides, *Science* **1996**, *273*, 347-349.

[8] X. M. Zhao, Y. N. Xia, G. M. Whitesides, *J. Mater. Chem.* **1997**, *7*, 1069-1074.

[9] E. Kim, Y. N. Xia, G. M. Whitesides, *J. Am. Chem. Soc.* **1996**, *118*, 5722-5731.

[10] Y. N. Xia, G. M. Whitesides, *Annual Review of Materials Science* **1998**, *28*, 153-184.

[11] J. C. McDonald, G. M. Whitesides, *Acc. Chem. Res.* **2002**, *35*, 491-499.

[12] a) J. C. McDonald, D. C. Duffy, J. R. Anderson, D. T. Chiu, H. K. Wu, O. J. A. Schueller, G. M. Whitesides, *Electrophoresis* **2000**, *21*, 27-40; b) M. K. Chaudhury, G. M. Whitesides, *Langmuir* **1991**, *7*, 1013-1025.

[13] M. J. Owen, P. J. Smith, *J. Adhes. Sci. Technol.* **1994**, *8*, 1063-1075.

[14] M. A. Unger, H. P. Chou, T. Thorsen, A. Scherer, S. R. Quake, *Science* **2000**, *288*, 113-116.

[15] Y. N. Xia, G. M. Whitesides, *Angew. Chem., Int. Ed.* **1998**, *37*, 551-575.

[16] E. Kim, Y. N. Xia, G. M. Whitesides, *Nature* **1995**, *376*, 581-584.

[17] a) P. G. de Gennes, *Rev. Mod. Phys.* **1985**, *57*, 827-863; b) M. Dong, F. A. L. Dullien, I. Chatzis, *J. Colloid Interface Sci.* **1995**, *172*, 21-36; c) P.-G. de Gennes, F. Brochard-Wyart, D. Quere, *Capillarity and Wetting Phenomena: Drops, Bubbles, Pearls, Waves*, Springer, **2004**.

[18] E. Kim, G. M. Whitesides, *J. Phys. Chem. B* **1997**, *101*, 855-863.

[19] W. F. Huang, Q. S. Liu, Y. Li, *Chem. Eng. Technol.* **2006**, *29*, 716-723.

[20] M. W. Davidson, A. Mortimer, *Encyclopedia of Imaging Science and Technology*, **2002**.

CHAPTER 3

Amyloid aggregation in confinement: mimicking effect of cell crowding in Alzheimer's Disease

This chapter describes the study of β-Amyloid 1-40 peptide aggregation at solid-liquid interface in a confined environment artificially created by means of unconventional fabrication techniques, and aimed to mimick the effect of the cell crowding.

3.1 Introduction

Degenerative diseases of the human brain have long been viewed as among the most enigmatic and intractable problems in medicine. As research on human neurodegeneration has moved from the descriptive phenomenology to the understanding of the mechanism, it has become increasingly apparent that the morphological lesions long used by neuropathologists to confirm a clinical diagnosis *post mortem* might provide an experimental handle to understand causative pathways. This findings have merged the study of neurodegenerative diseases with a more restricted area of medicine, the study of amyloidosis. Amyloids were defined some 150 years ago as tissue deposits of extracellular filaments (usually called fibrils) that were microscopically, and in severe cases macroscopically, visible in various organs in several seemingly unrelated human diseases. In the twentieth century, it was found that amyloid fibrils were proteinaceous in origin, and by the 1960s some amyloid sub-units, such as the fragments of immunoglobulin that accumulate in certain immune-related amyloidosis, were identified as specific proteins. Biochemical and ultra-structural experiments established the insolubility of amyloid fibrils in aqueous buffers. X-ray-diffraction analyses on purified fibrils indicated that the constituent proteins were un usually rich in highly ordered, β-pleated sheet structure, providing an apparent explanation for their long-known property of binding to the histochemical dye Congo red in a polarized manner. These advances in elucidating amyloid deposits in peripheral tissues encouraged amyloidologists to apply their methods to neurodegenerative disorders, most not ably with the seminal studies in 1984 of Glenner on the cerebrovascular amyloid deposits of Alzheimer's disease (AD). As research on the protein deposits of AD grew increasingly intensive, similar concepts and methods began to be applied to other human neurodegenerative disorders.

AD is a devastating, fatal, neurological disorder with no known cause and no cure. It is primarily an age-related disease, and it has become a very serious problem as the general life-expectancy is gradually increasing. AD is the most common neurodegenerative disease, directly affecting about 10% of humans by age 65 and about 50% by age 85[1]. The average period of survival is 8 years after diagnosis. The afflicted person suffers progressive loss of memory and cognitive ability, mood swings, personality changes, and loss of independence. AD is accompanied by three main structural changes in the brain[2]: (i) diffuse loss of neurons; (ii) intracellular protein deposits (the

neurofibrillary tangles, NFT) consisting of phosphorylated tau protein; and (iii) extracellular protein deposits (amyloid (Aβ) or senile plaques) surrounded by dystrophic neurites.

Based on these neuropathological markers, two major hypotheses were initially proposed. (i) According to the amyloid cascade hypothesis[3], neurodegeneration in AD begins with the abnormal processing of the amyloid precursor protein (APP) and results in the over-production, aggregation, and deposition of the Aβ peptide[4]. Apparently, the amyloid cascade may facilitate NFT formation and cell death. (ii) According to the neuronal cytoskeletal degeneration hypothesis, cytoskeletal changes are the main events that lead to neurodegeneration in AD, as the hyperphosphorylation and aggregation of tau are related to the activation of cell death processes[5]. That Aβ is a causative agent in AD, first enunciated as the amyloid hypothesis is now widely accepted[4, 6]. Elucidation of the mechanism of Aβ aggregation is crucial to understanding the progression of the disease, and possibly intervene on it at the early stages.

THE AMYLOID β-PEPTIDE (Aβ)

The Aβ peptide is a normal, soluble component of human plasma and cerebrospinal fluid[7]. It is toxic only after it undergoes aggregation and/or conformational changes to produce oligomers or fibrils[8].

Aβ is generated intracellularly by the proteolytic processing of APP, a glycosylated transmembrane protein, by two proteases known as β- and γ-secretase[9]. A third secretase, α-secretase, cleaves the Aβ sequence itself and is therefore usually considered as non-amyloidogenic. A view of cleavage sites and membrane spanning of APP is given in Figure 3.1[10]. α-Secretase and β-secretase cleave the ectodomain of APP, resulting in the shedding of APPsα and APPsβ. γ-Secretase finally cleaves the transmembrane domain of the APP carboxy terminal fragments, releasing the Aβ peptide into the extracellular milieu and the APP intracellular domain into the cytoplasm. The strongest evidence that abnormal proteolytic processing and increased Aβ generation are central to the disease process comes from studies of very rare inherited forms of AD[11].

The main alloforms of Aβ are 40 and 42 amino acids long, both of which are disease associated. Despite the small structural difference between Aβ1-40 and Aβ1-42, they display distinct clinical, biological, and biophysical behavior. Some studies have shown that Aβ1-40 and Aβ1-42 self-

assemble via different pathways[12]. The Aβ1-42 dodecamer is a candidate for the primary toxic species in AD. Instead, Aβ1-40 does not form paranuclei, but existed as a mixture of monomers, dimers, trimers and tetramers (Figure 3.2)[13]. Aβ1-40 is the dominant peptide species in human cerebrospinal fluid according for approximately 90% of total Aβ under normal conditions[14].

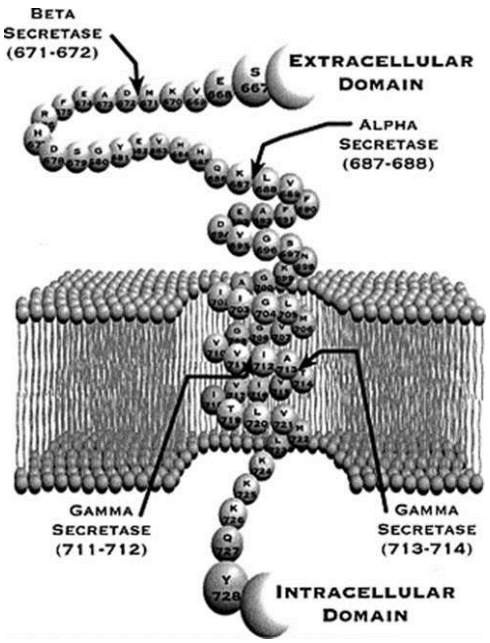

Figure 3.1 Schematic view of the membrane spanning and cleavage sites of APP770. The Aβ1-40 fragment, generated by β- and γ-cleavage, comprises residues 672-711 of APP770 while the Aβ1-42 fragment spans residues 672-713.

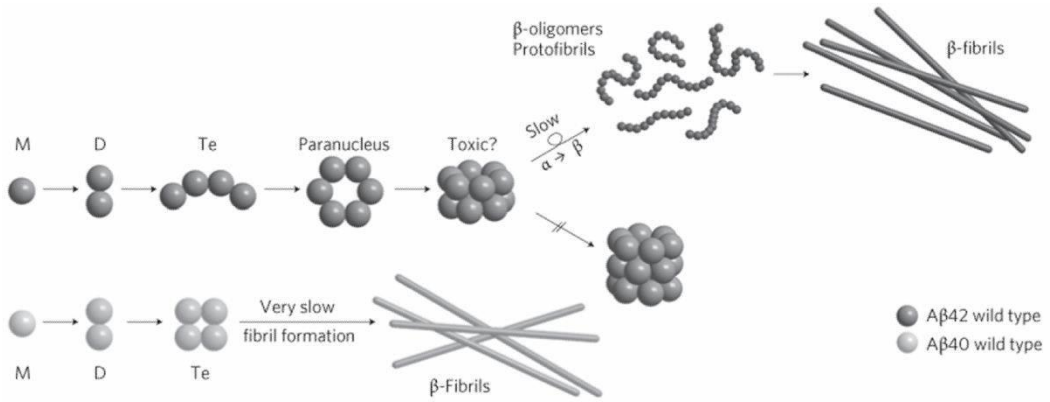

Figure 3.2 Schematic mechanism of oligomerization and fibril formation for Aβ1-42 and for Aβ1-40. For Aβ1-40 the key structure is the tetramer that resists further monomer or dimer addition. In Aβ1-42 an "open" tetramer promotes the formation of the planar hexamer (paranucleus) and the stacked dodecamer, which resists further reaction.

3.2 β-Amyloid 1-40 peptide aggregation at solid-liquid interface in confinement

INTRODUCTION

Elucidating the factors which might trigger the nucleation of the small stable oligomers of Aβ peptide and their growth into fibrils, bundles and plaques at later times[15] is crucial for identifying possible therapeutic targets[4, 12b, 13].

The role of environmental factors, including temperature, pH, shear flow, ionic strength, pressure, as well as the presence of metal ions or small molecules, has been largely investigated in the process of Aβ aggregation[16]. Most of the earlier experimental and computational investigations were performed in homogeneous, bulk conditions, although the actual cellular environment is much more complex. Fibril forms at biological membrane *in-vivo*. The detailed investigation of the events occurring on the surface of lipid membranes, although needed, is hindered by the heterogeneity and experimental complexity of the cell membrane, which often makes difficult data interpretation. Surfaces with well-defined chemical and physical properties can be conveniently used as prototype systems to study the effect of surface properties on amyloid adsorption, nucleation, aggregation and fibril formation[17]. The interest towards protein aggregation on surfaces has grown substantially[18] also due to the robust technological control of materials surfaces and bio-interfaces achieved with nanotechnology on biomedical devices[19].

Another feature of the cell environment is crowding[20]. A limited number of studies pointed out the effect of geometrical confinement on fibril formation and protein folding[21]. The confinement might affects conformational changes in proteins leading to irreversible aggregation[22] which hinders the protein functionality and might lead to the formation of toxic species. Cell membrane and crowding define a confined environment where amyloidosis occurs. Pathological conditions might indeed involve a change in the local surface tension of the extracellular membrane, for instance due to a change in the local protein content, curvature or rigidity. In many systems where amyloidosis occurs, the role of specific interface and the effect of cellular crowding should be addressed in order to draw correct hypothesis on the mechanism associated to the pathology of AD.

Studying these effects requires the technological control of size, dimensionality, interfacial chemistry, and rheology of the confined solutions of Aβ. Microfluidics technology is a robust platform for investigating the aggregation of Aβ peptide in micro- and mesoscopic channels.

Confinement affects the kinetics of the aggregation by decreasing the diffusion time scale of molecular and oligomeric species. Moreover, the surface interactions compete with the intermolecular interactions in the solution, by altering the energy barriers for nucleation of the stable oligomers, and hence modulating the lag time[21b, 23].

The study of the Aβ1-40 peptide aggregation in confinement addresses the influence of the surface tension in confined environment on the aggregation of this peptide *in-vitro*. The aim of this work is to understand how the early stages of aggregation of Aβ1-40 peptide is influenced by the proximity of an interface between the solution and the solid surface. Microfluidics allows us to accurately control the local concentration of Aβ1-40 peptide throughout incubation time up to hundreds of hours[23a],which is important for guaranteeing reproducible conditions. A systematic change of the surface tension of the walls of the microfluidics channels has been carried out.

EXPERIMENTAL SECTION

The Aβ1-40 peptide was purchased from Sigma-Aldrich (A1075) and it was dissolved in ultrapure water to reach the concentration of 6 μM (corresponding to 25 μg/mL), which corresponds to a strongly pathological value[24]. The solvent chosen was water and not a physiological media because of the high solubility of the peptide in this solvent, and the absence of salts facilitates the AFM characterization.

We use MIMICs (see Chapter 2.4) to confine, for two hours, the Aβ1-40 peptide solution within the mesoscopic channels defined by the PDMS stamp protrusions sealed to the oxidized surface of a silicon wafer (Figure 3.3).

When the solution is placed at an open end of the stamp, the solution with surface tension γ_{LV} spontaneously in-fills the channels forced by the Laplace pressure[25]:

$$\Delta P = 2\gamma_{LV} \cos\theta / r \ .$$

The contact angle θ is defined by Young's equation:

$$\cos\theta = (\gamma_{SV} - \gamma_{SL}\ )/\gamma_{LV} \ .$$

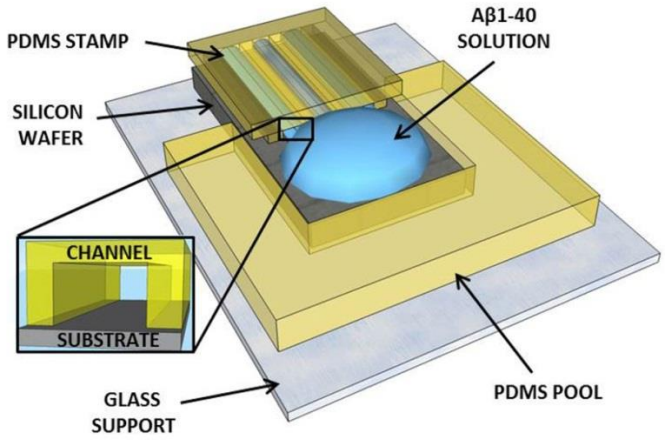

Figure 3.3 Schematic representation of the experimental set-up with a detail of a channel.

The surface tensions γ_{SV} and γ_{SL} refer to the substrate and the channel walls, r is the effective diameter of the channel[26].

In this experiment, we control the surface tension of the PDMS walls by means of an air plasma treatment. We adjust the time between the treatments of PDMS and silicon wafer in such a way that they exhibit the same contact angle by the time they are sealed one onto the other. In this manner, the surface tension of the solid-liquid interface γ_{SL} is homogeneous inside the channel, and no pinning or turbulence is created. We also assume that, owing to minor topography effects (both PDMS and SiO_2 are smooth surfaces, with maximum RMS roughness below 0.5 nm) the Aβ peptides adsorbing on the surface will experience mostly the chemical component of the surface tension.

The PDMS stamp, obtained by Replica Molding (see chapter 2.3), consists of an array of parallel channels whose width and height are 900 nm and 200 nm, respectively, and the pitch (inter channel distance) is 1.5 µm. As-casted PDMS is highly hydrophobic, so an air plasma treatment for 1 min at 30 mA by Glow discharge Cleaning System (Pelco, easiGlow™) was performed in order to make the stamp hydrophilic. PDMS tends to recover its original hydrophobicity in time (squares in Figure 3.4). The surface employed for this study is silicon wafer (n-type doped, supplied by FBK, Trento Italy) with a 200 nm thermally grown SiO_2 layer on the top. The wafer is first cleaned with acetone and Piranha solution (1:1) to remove the protective photoresist layer, then immersed in HF (2%) for 5 seconds in order to partially etch the thermal oxide. The result is a hydrophilic silicon oxide that recovers its original surface tension in about one week (circles in Figure 3.4). Therefore, the surface tension of the confinement is modulated by sealing the stamps

at different timings after the plasma treatment to the silicon substrate. We choose the appropriate time-lag for the processing of PDMS in order to match both surface tensions. Figure 3.4 shows that PDMS and Si wafer have different recovery timescales.

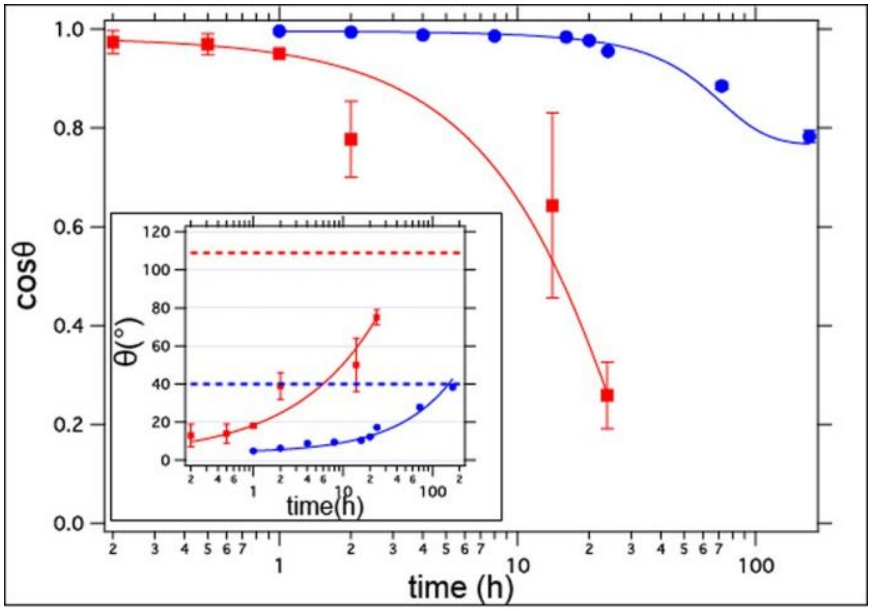

Figure 3.4 Recovery of the surface tension (proportional to cosθ) for PDMS (squares) and silicon oxide (circles) after the cleaning procedure. Continuous lines are weighted fit with a sigmoid function, whose long time limit is the contact angle prior treatment. Inset: time evolution of the contact angle θ, continuous lines are power law fits.

AFM CHARACTERIZATION

The stamp was placed onto the silicon substrate and a 30 μL droplet solution was deposited on the open end of the stamp and allowed to dry over after 2 hours in air at room temperature. During this time, owing to the values of contact angles between 10° and 40°, we are sure that the channel has been completely infilled by the solution. The stamp was gently removed and the sample was scanned by AFM in air once completely dried. AFM images were acquired with a stand-alone SMENA NT-MDT microscope operated in semi-contact mode under ambient conditions, using Si_3N_4 cantilever (NSG 11, NT-MDT) with a resonant frequency 150-250 kHz, force constant 5-10 N/m and a typical tip curvature radius of 10 nm.

AFM shows the evolution of the morphology of the aggregates corresponding to a variation of the surface tension inside the nanometric channels. Upon increasing the contact angle of the

channel walls, the peptide aggregates change their morphology from lines, to thin films, to droplets (Figure 3.5).

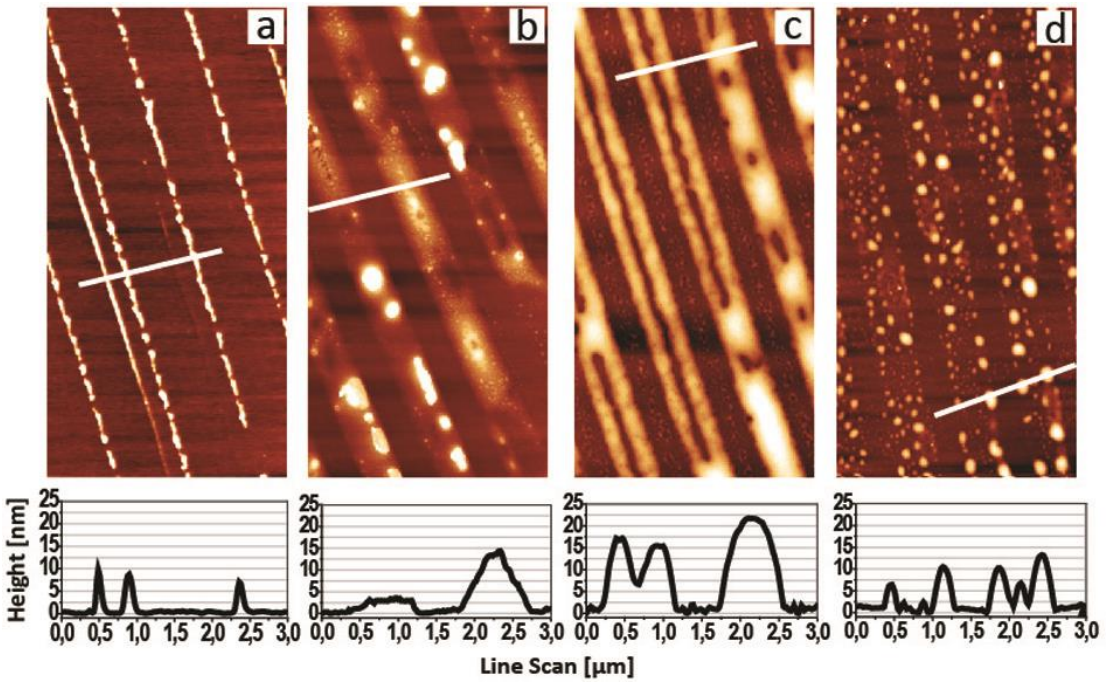

Figure 3.5 Typical AFM images of Aβ1-40 (6 µM) patterned on a silicon surface with different contact angles: (a) 10°, (b) 20°, (c) 30° and (d) 40°. All images are 5x10 µm. Below are shown corresponding height profiles perpendicular to the channels

When the contact angle of the channels is θ=10° the aggregates consisted of narrow aligned lines, (Figure 3.5a) pinned to the channel edges. They appear formed by coalescence of shorter segments, with an average height of 10nm. At θ=20°, small globular dots form on top of a first monolayer covering the whole area of the channels (Figure 3.5b). At θ =30° the layer dewets by hole nucleation, growth and coalescence. At the bottom of the holes the first monolayer is still visible, hinting to self-dewetting. On top of the film, larger aggregates form (Figure 3.5c). At θ=40° the wetting of the channel by a film is completely prevented, and only globular aggregates with different height are observed (Figure 3.5d). Some aggregates coalesce giving rise to larger droplets. This evidence suggests that the deposits wet the surface at a contact angle of 10°, dewet at contact angles above 20°, and nucleate and grow in a partial wetting regime above 30°.

RESULTS AND DISCUSSION

We attempt to rationalize the influence of surface tension on the morphology of the aggregates by the analysis of the AFM images. We used the open source image software Gwyddion (www.gwyddion.net) and in particular the volume of each aggregate was analyzed by the Grain Analysis function. The total volume deposited per unit area is plotted in Figure 3.6 *vs.* cosθ. The data exhibit a concave parabolic trend, which separates a regime of wettability at high cosθ values from a region of globular aggregation at lower values . Noticeably, there is a surface tension window near cosθ=0.85 which maximizes the amount of deposited material.

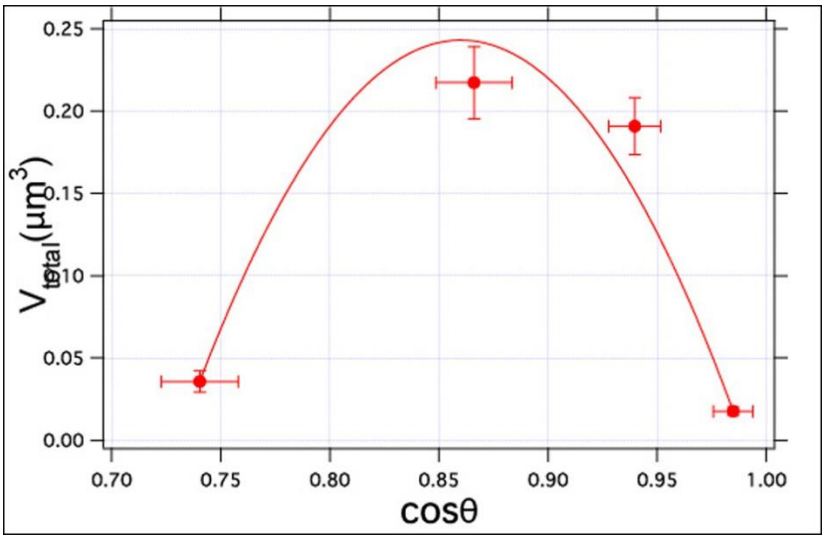

Figure 3.6 Total volume of the deposit vs. surface tension proportional to the contact angle. Continuous line is a parabolic fit with weights given by the standard deviation.

The observation of a surface tension affecting the deposition of Aβ peptide in the microfluidics channels can be analyzed by mass transport phenomena occurring in the MIMICs system. Despite of its apparent simplicity, MIMICs is complicated by a series of concurrent or competing transport phenomena. The surface tension affects (i) the flow of the solution in the channel, (ii) the nucleation and growth rate of the aggregates on the silicon oxide surface, (iii) the evaporation rate of the droplet pinned to the MIMICs pool.

In the case (i) the Laplace pressure is modulated by the square root of the surface tension. The channels are filled with the solution within fractions of seconds. Owing to the weak dependence

and the range of cosθ spanned in the experiment (in our case from 0.75 to 1), we believe that there is not a substantial change in the infilling velocity.

Nucleation and growth rates (ii) depend on: - the deposition rate of the peptide from the solution to the surface, - the peptide diffusivity across the surface, and - the nucleation free energy on the surface. The peptide molecules diffuse in the solution to the surface according to the peptide concentration in the channel. The concentration depends on the surface tension and changes in time and along the length of the microchannel. The effective deposition rate results from the balance between the molecular diffusivity in solution and the adsorption and desorption rates. The latter depend on the energy barriers associated to the conformational changes required for establishing stable/unstable interaction of the peptides on the surface, and hence depend on surface tension. Once the molecules are adsorbed, they explore the surface by diffusing across, before a steady anchoring point, such as a nucleus or a defect, is found. Surface tension modulates the mean free path of the peptide molecules on the surface and the nucleus density, thus determining the supersaturation condition[27], the deposition rate at which stable nuclei are formed on the surface, and ultimately, the size and dimensionality of stable nuclei.

About the concentration of the peptide solution in the channel, its initial value equals that of the solution because of the capillary flow. At timescales longer than a few seconds, concentration decreases because of the adsorption, whereas is partially replenished by surface desorption and by the molecular diffusion from the outer reservoir to inside the channel. The time-varying concentration gradient created from the outside to the inside of the channel is the driving force of the diffusion of peptides from the pool inside the channel.

Two opposite phenomena determine the peptide concentration in the droplet in the pool, and hence the gradient. The water evaporation rate (iii) is larger when surface tension of the silicon wafer is smaller, and hence concentration increases faster. Conversely, concentration decreases as peptide is deposited within the pool. The scenario is further complicated by the fact that concentration profile in the pool is not constant both in time and across the pool. The drop of solution is pinned to the edge of the PDMS stamp due to the capillary force. Due to water evaporation, it recedes from the edge of the three-phase line towards the edge of the PDMS stamp producing the so-called coffee-stain effect[28]. This convective flow towards the entrance of the MIMICs channel increases peptide concentration near the entrance and leads to a variety of phenomena outside the channels, like oligomerization, aggregation and fibrillation in the solution

or the surface. As a consequence, peptide aggregates precipitate before entering the channel. This is a main cause for the non-conserved mass deposited inside the channels.

About the nature of aggregates, we observed the absence of well-defined Bragg-peaks when GIXD is performed on the deposits at the various angles along the parallel lines. This suggests that the deposited aggregates are in an amorphous, glassy state, rather than a beta-sheet amyloid state, hinting that reduction of either the spatial degrees of freedom or shortening of the timescales of deposition prevent the peptides to re-arrange their conformation or find the proper structural stacking relations.

3.3 Conclusions

In conclusion, we showed that the morphology and the size of the Aβ1-40 aggregates depend on the surface tension inside the channels of a microfluidics. By increasing the contact angle of the channel from 10° to 40° the aggregate forms change from thin films to droplets, as in a wetting/dewetting transition of a polar material. Our interpretation is given in terms of a progressive change of the kinetic mechanism of aggregation, due to the interplay between diffusion and capillary flow. At 10° contact angle, the effective deposition rate in the channel is slow (rate determining step) with respect to the diffusion from the pool to the channel and inside the solution. At 40° contact angle, the effective deposition rate is high and the diffusion from the pool to inside the channel is slow (rate determining step). Both occurrences yield a massive deposition outside the channel. At 20° and 30° the diffusion and deposition rates are comparable and they result in more material entering the channels and being deposited there. In control experiments in bulk solutions, fibrils deposited on the substrate were observed at comparable timescales of incubation.

Our results highlight the possible role of the local surface energy and size confinement in altering the aggregation pathways and timescales of amyloid peptides. Cell membrane and crowding define a confined environment where amyloidosis occurs. Pathological conditions might indeed involve a change in the local surface tension of the extracellular membrane, for instance due to a change in the local protein content, curvature or rigidity. In many systems where amyloidosis occurs, the role of specific interface and the effect of cellular crowding should be addressed in

order to draw correct hypothesis on the mechanism associated to the pathology of Alzheimer's disease.

Bibliography

[1] H. N. Fillit, A. W. O'Connell, W. M. Brown, L. D. Altstiel, R. Anand, K. Collins, S. H. Ferris, Z. S. Khachaturian, J. Kinoshita, L. Van Eldik, C. F. Dewey, *Alzheimer Disease & Associated Disorders* **2002**, *16*, S1-S8.

[2] F. Torreilles, J. Touchon, *Progress in Neurobiology* **2002**, *66*, 191-203.

[3] G. G. Glenner, C. W. Wong, *Biochem. Biophys. Res. Commun.* **1984**, *122*, 1131-1135.

[4] J. Hardy, D. J. Selkoe, *Science* **2002**, *297*, 353-356.

[5] G. V. De Ferrari, N. C. Inestrosa, *Brain Research Reviews* **2000**, *33*, 1-12.

[6] a) F. M. LaFerla, K. N. Green, S. Oddo, *Nat. Rev. Neurosci.* **2007**, *8*, 499-509; b) W. Q. Qiu, M. F. Folstein, *Neurobiology of Aging* **2006**, *27*, 190-198; c) L. M. Sayre, M. G. Zagorski, W. K. Surewicz, G. A. Krafft, G. Perry, *Chem. Res. Toxicol.* **1997**, *10*, 518-526; d) D. J. Selkoe, *Jama-Journal of the American Medical Association* **2000**, *283*, 1615-1617.

[7] a) M. Pitschke, R. Prior, M. Haupt, D. Riesner, *Nat. Med.* **1998**, *4*, 832-834; b) P. Seubert, C. Vigopelfrey, F. Esch, M. Lee, H. Dovey, D. Davis, S. Sinha, M. Schlossmacher, J. Whaley, C. Swindlehurst, R. McCormack, R. Wolfert, D. Selkoe, I. Lieberburg, D. Schenk, *Nature* **1992**, *359*, 325-327.

[8] a) C. J. Pike, A. J. Walencewicz, C. G. Glabe, C. W. Cotman, *Brain Res.* **1991**, *563*, 311-314; b) C. J. Pike, D. Burdick, A. J. Walencewicz, C. G. Glabe, C. W. Cotman, *J. Neurosci.* **1993**, *13*, 1676-1687; c) L. K. Simmons, P. C. May, K. J. Tomaselli, R. E. Rydel, K. S. Fuson, E. F. Brigham, S. Wright, I. Lieberburg, G. W. Becker, D. N. Brems, W. Y. Li, *Mol. Pharmacol.* **1994**, *45*, 373-379.

[9] D. J. Selkoe, *Physiological Reviews* **2001**, *81*, 741-766.

[10] P. R. Turner, K. O'Connor, W. P. Tate, W. C. Abraham, *Progress in Neurobiology* **2003**, *70*, 1-32.

[11] J. Hardy, *Neurobiology of Aging* **2002**, *23*, 1073-1074.

[12] a) G. Bitan, A. Lomakin, D. B. Teplow, *J. Biol. Chem.* **2001**, *276*, 35176-35184; b) G. Bitan, S. S. Vollers, D. B. Teplow, *J. Biol. Chem.* **2003**, *278*, 34882-34889.

[13] S. L. Bernstein, N. F. Dupuis, N. D. Lazo, T. Wyttenbach, M. M. Condron, G. Bitan, D. B. Teplow, J.-E. Shea, B. T. Ruotolo, C. V. Robinson, M. T. Bowers, *Nature Chem.* **2009**, *1*, 326-331.

[14] G. C. Gregory, G. M. Halliday, *Neurotoxicity Research* **2005**, *7*, 29-41.

[15] a) W. K. Serem, C. K. Bett, J. N. Ngunjiri, J. C. Garno, *Microscopy Research and Technique* **2011**, *74*, 699-708; b) A. Rauk, *Dalton Trans.* **2008**, 1273-1282; c) J. Adamcik, J.-M. Jung, J. Flakowski, P. De Los Rios, G. Dietler, R. Mezzenga, *Nat. Nanotechnol.* **2010**, *5*, 423-428.

[16] a) C. L. Shen, R. M. Murphy, *Biophys. J.* **1995**, *69*, 640-651; b) B. Morel, L. Varela, A. I. Azuaga, F. Conejero Lara, *Biophys. J.* **2010**, *99*, 3801-3810.

[17] B. Moores, E. Drolle, S. J. Attwood, J. Simons, Z. Leonenko, *PLoS One* **2011**, *6*.

[18] a) A. Nayak, A. K. Dutta, G. Belfort, *Biochem. Biophys. Res. Commun.* **2008**, *369*, 303-307; b) A. Sethuraman, G. Belfort, *Biophys. J.* **2005**, *88*, 1322-1333; c) G. B. Sigal, M. Mrksich, G. M. Whitesides, *J. Am. Chem. Soc.* **1998**, *120*, 3464-3473.

[19] F. Valle, B. Chelli, M. Bianchi, P. Greco, E. Bystrenova, I. Tonazzini, F. Biscarini, *Advanced Engineering Materials* **2010**, *12*, B185-B191.

[20] a) A. B. Fulton, *Cell* **1982**, *30*, 345-347; b) S. B. Zimmerman, S. O. Trach, *J. Mol. Biol.* **1991**, *222*, 599-620; c) R. J. Ellis, *Trends Biochem. Sci.* **2001**, *26*, 597-604.

[21] a) J. Kraineva, V. Smirnovas, R. Winter, *Langmuir* **2007**, *23*, 7118-7126; b) J. Mittal, R. B. Best, *Proc. Natl. Acad. Sci. U. S. A.* **2008**, *105*, 20233-20238.

[22] F. Librizzi, V. Fodera, V. Vetri, C. Lo Presti, M. Leone, *European Biophysics Journal with Biophysics Letters* **2007**, *36*, 711-715.

[23] a) P. Dejardin, E. N. Vasina, in *Principles and Practice, Proteins at Solid-Liquid Interfaces* (Ed.: P. Dejardin), Springer-Verlag, Berlin Heidelberg, **2006**, pp. 51-73; b) D. Homouz, M. Perham, A. Samiotakis, M. S. Cheung, P. Wittung-Stafshede, *Proc. Natl. Acad. Sci. U. S. A.* **2008**, *105*, 11754-11759.

[24] J. D. Harper, P. T. Lansbury, *Annu. Rev. Biochem.* **1997**, *66*, 385-407.

[25] P.-G. de Gennes, F. Brochard-Wyart, D. Quere, *Capillarity and Wetting Phenomena: Drops, Bubbles, Pearls, Waves*, Springer, **2004**.

[26] E. Kim, Y. N. Xia, G. M. Whitesides, *J. Am. Chem. Soc.* **1996**, *118*, 5722-5731.

[27] S. Verlaak, S. Steudel, P. Heremans, D. Janssen, M. S. Deleuze, *Physical Review B* **2003**, *68*.

[28] R. D. Deegan, O. Bakajin, T. F. Dupont, G. Huber, S. R. Nagel, T. A. Witten, *Nature* **1997**, *389*, 827-829.

CHAPTER 4

Multiscale gradient functionalization with amphiphilic cyclodextrin for tumor cell recognition

In this chapter, the functionalization of a glass substrate with amphiphilic cyclodextrin bearing different cues as a method to study the effect of local topography on cell adhesion and growth is shown.

4.1 Introduction

The control of the cell environment is crucial to many aspects of cell research and medical applications. Observed changes in gene expression profile of primary cells *in-vitro* compared to that of cells in the organ raised serious concerns in the pharmaceutical industry, because drug-screening technology is largely based on cell culture data. Regenerative medicine requires control of stem cell commitment at the level of individual cells and colonies *in-vitro*. Other applications where the control of cell environment would be desirable include diagnostics; loco-regional therapy of neurological diseases; sorting and localization of cancer cells before metastasis occurs. Cell behavior is influenced by the 3D-environment dynamically sensed by the cell[1]. This involves topo-chemical-mechanical stimuli, electromagnetic fields, gradients of chemo-attractants, haptotaxis[2]. In order to mimic the environment of the cells in an organ it is necessary to control cell-cell contacts and communication [3]. The exchange of nutrients, metabolites and signals across the different interfaces must be guaranteed. This requires a spatial and dimensional control of the structures composing the environment in addition to a temporal control of the cues interacting with the cells.

Investigation of selected cues highlighted the importance of topographical, chemical, and more recently mechanical/viscoelastic interactions of the cell and the surface[4]. Albeit the proofs-of-concept have been demonstrated, important questions related to the complexity of the cell environment remain still at an infancy level: what is the effect of combined cues? Is there synergy or competition between different cues? How can cell behavior on a surface be reprogrammed by a dynamic change of the environment (e.g. adhesion or detachment upon switching interfacial energy)? Are there correlations among different cues? How does the cell fate emerges from combined cues? Other important aspects concern the adhesion and the migration driven upon the environmental stimuli. These questions call for a technology platform of greater complexity that is not currently available, where topo-chemical and mechanical cues are modulated in space and time. It should comprise devices to probe and stimulate cells. Device integration is routine on wafers, but is still challenging on transparent flexible substrates. Micro-fabrication and unconventional approaches enable the integration of functional materials to sub-micrometer scale feature size[5].

Our research activity here is part of the European Science Foundation (ESF) project Intelligent Cell Surfaces (ICS). The vision is a bio-mimicking breadboard designed for quantitative studies

of cell response (in terms of motility, adhesion, self-aggregation, functionality, differentiation) to external stimuli in time and space. The breadboard is engineered with sensing units for measuring signals and inducing stimuli, and actuating devices and structures for directing the motion of the different cell types. The development of such a breadboard requires the integration of multidisciplinary competences: bio-hybrid materials and interfaces, self-organization phenomena, thin films, patterning and multiscale fabrication, microfluidics, scanning probe microscopies, nanoscale optics, organic electronics, neurobiology.

The design of microenvironments suitable to integrate cells in implantable devices, to build cell-based biosensors[6],or control the delivery of molecules for therapy and diagnosis[7], require an understanding on how the different cues should be presented to the cells in space and time. Cyclodextrines (CyD) represent a versatile chemical toolbox that can be reconfigured for different types of cues, can be processed by a variety of unconventional techniques, and can be chemically-physically modulated or tailored by means of gradual changes in the environment, for instance by inducing changes in size, aggregation, spreading of the vesicles they form. The stabilization in solution of CyD allows us to use them for surface functionalization or coating. A new generation of amphiphilic cyclodextrins (ACyD) modified with thioalkyl groups on the upper rim and oligoethylene-glycolon the lower rim[8] are good candidates for these applications. They are prototype water-soluble carriers endowed with a variety of terminal groups. A. Mazzaglia et al. have demonstrated that especially designed ACyD are capable of forming micellar aggregates[8b, 9] or vescicles[8a, 8c] of potentially low immunogenity due to their oligo(ethyleneglycol) exterior[10]. They are more versatile as drug encapsulators than individual CyD molecules and are building blocks for ultra-thin layers as they can be fused on surface by tuning surface tension.

CYCLODEXTRINS

Supramolecular chemistry involves non-covalent interactions, such as hydrogen bonds, hydrophobic interaction, metal coordination, dipole interactions, van der Waals interactions, electrostatic forces, among the interacting species. Most of supramolecular interactions involve host-guest assemblies. Among potential hosts, CyDs play an important role, for the following reasons[11]:

(1) They are semi-natural products, produced from a renewable natural material, starch, by a relatively simple enzymatic conversion.

(2) They can be produced in large amounts by environmentally friendly technologies and at low cost.

(3) Properties of the complexed substances can be modified significantly by the inclusion. This "supramolecular encapsulation" is widely exploited in industrial products, technologies, and analytical methods.

(4) Potential toxic effects can be mitigated or eliminated by selecting the appropriate CyD type or derivative or mode of application.

(5) As a result of point 5, CyDs can be consumed as ingredients of drugs, foods, or cosmetics.

The three major CyDs are crystalline, homogeneous, non-hygroscopic substances, which are torus-shaped macro-rings built up from glucopyranose units. The α-CyD comprises six glucopyranose units, β-CyD comprises even such units, and γ-CyD comprises eight such units (Figure 4.1). In an aqueous solution, the slightly apolar CyD cavity is occupied by water molecules which are energetically un-favored (polar-apolar interaction),and therefore can be readily substituted by appropriate "guest molecules" which are less polar than water. Their properties as molecular hosts[12], their multifunctionality[13] and their unusual adaptability as oligosaccharides to selective modification[14] make them unique mesomolecular objects for chemical biology. For this reason, one of the aim of this study, is to use molecules and precursors as chemical cues for cells to follow, adhere and proliferate.

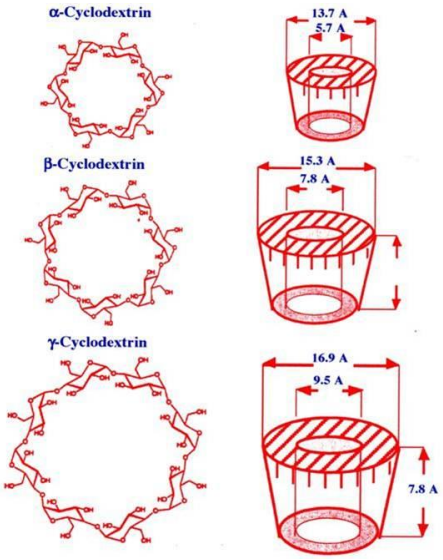

Figure 4.1 Molecular Structure of α, β, and γ cyclodextrins.

4.2 Amphiphilic cyclodextrin pattern by MIMICs

The synthesis of ACyD used in this study was performed by the group of Dr. A. Mazzaglia in CNR-ISMN Messina. It was carried out by covalent grafting of hydrophobic and hydrophilic group on the narrow and wide rim of the cyclodextrin cavity, respectively. The macrocycle was tailored by appending groups that either yield stability ACyD, and targeting groups that increase selectivity. In particular, the upper ring was modified with thioalkyl groups ($-SC_{16}H_{33}$) and the lower rim with polyethylene glycol chain (PEG) bearing terminal –OH, $-NH_2$ and mannose ligand groups (Figure 4.2).

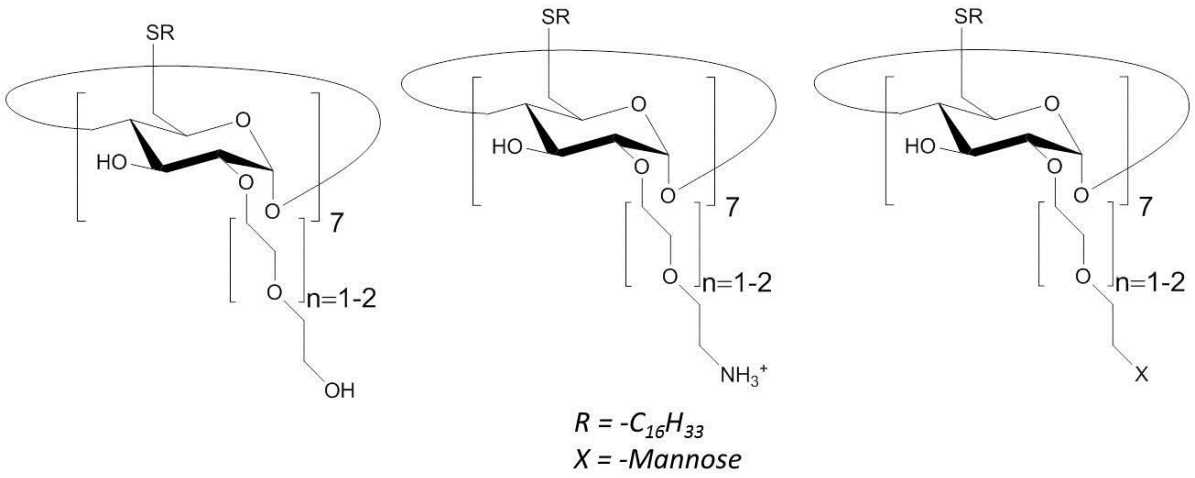

Figure 4.2 Sketched structure of the investigated ACyD.

For targeting a specific type of cells, ACyD shave been synthesized with a group that interact specifically with a receptor over-expressed by those cells. ACyD with NH_2 group at the end of PEG moiety can interact favorably with cell membrane; ACyD with terminal OH groups acts as antifouling cue, and can be patterned for restricting the area occupied by the cell and therefore for guiding the cells towards specific regions where they can adhere. Mannose was chosen as targeting epitopes since it interacts with receptors present on a number of tumor cells. For example, it has been demonstrated[15] that mannosylated bovine serum albumin is efficiently taken up by liver non-parenchymal cells, mainly composed of sinusoidal endothelial cells and Kupffer cells, after intravenous injection.

ACyD solution was prepared from a stock solution (1 mg/mL) in dichloromethane, which was slowly evaporated under a steam of N_2 to form a thin film. The film was again solubilized in CH_2Cl_2 (Figure 4.3a) and after the complete solvent evaporation (Figure 4.3b), it was hydrated to

reach the concentration of 0.1 mg/mL (Figure 4.3c). It was maintained at 60°C for 1h and sonicated for 1.5 h. The ACyDs have poor water solubility, in fact a suspension of aggregates is obtained in water. It is stable for 3 weeks and it is necessary to sonicate the solution before each experiment.

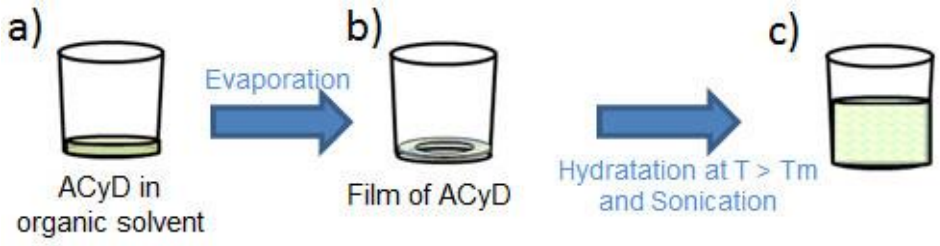

Figure 4.3 Experimental steps involved inthe ACyD solution restoring.

For patterning ACyDs we use MIMICs (see Chapter 2.4) with a PDMS stamp which confines the ACyD solution within the channels defined by the PDMS stamp protrusions in intimate contact with the substrate (Figure 4.4a).

The master used for PDMS replica consists of protruding lines that become grooves in the replica. When the PDMS stamp is placed in contact with the surface, the grooves form the channels. When the solution is poured at an open end of the stamp it spontaneously in-fills the channels. Depending on the solute, precipitation, aggregation, or self-organization occurs at the later stage of the solvent evaporation.

We patterned ACyD on glass for facilitating the imaging of cells afterwards. A glass slide (THERMO Scientific Menzel-Glaser) was cleaned with ethanol and dried with nitrogen, and characterized by AFM (Figure 4.4b) and contact angle after the cleaning procedure. We found that contact angle was 24°±1°.

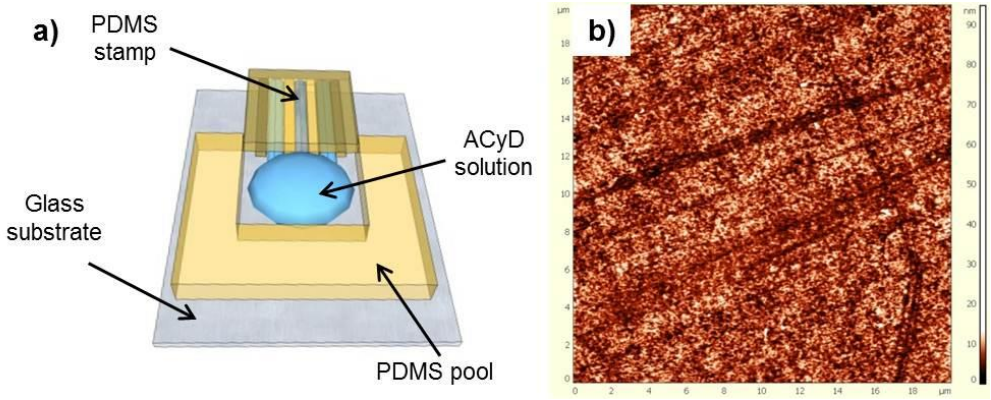

Figure 4.4 (a) Schematic representation of our experimental set-up; (b) typical AFM image (20x20 µm) of the glass substrate after the cleaning procedure.

The PDMS stamp, obtained by Replica Molding (see chapter 2.3), consists of an array of parallel channels whose width and height are 10µm and 3µm, respectively, and the inter channel distance is 25 µm.

We fabricated the photolithography mask by ablating a Ag film on a mirror glass using a CAD–driven Multifunction Laser Marker *ScribaR* (Scriba Nanotecnologie Srl, Bologna Italy) (Figure 4.5). *ScribaR* allows direct fabrication, writing and rapid prototyping without masks of a variety of objects with micrometer features, such as printed circuits, microfluidics, resists, masters, contact shadow masks, patterned thin films. The laser marker can work with a variety of materials, shapes and size of substrates. The laser beam path and a precision laser machining and positioning controlled by linear motors and coaxial camera allows for re-alignment when multiple fabrication steps are required. The feature size and the resolution can be as small as 5 microns.

Figure 4.5 External view (on the left) and internal view (on the right) of the multifunction laser marker *ScribaR*.

In order to control the deposition and organization of ACyD in MIMICs conditions, the concepts explored in Chapter 3 about the modulation of surface tension and its influence on the deposition mechanism in micro-channels have been adapted here. Two different experiments of patterning were performed.

The first is a controlled deposition of ACyD on glass surface by MIMICs in micrometer channels without performing any chemical treatment of the PDMS stamp. PDMS and glass have two different contact angles (Figure 4.6) so the ACyD solution cannot infill the whole channel length. As evident from the optical image (Figure 4.7a), we were not able to obtain a uniform pattern and we observed substantial amounts of ACyD deposits outside the channels. We characterized the pattern by AFM (Figure 4.7b,c). All data were acquired in air, using a SMENA NT-MDT scanning probe microscope, in tapping mode and using silicon cantilever.

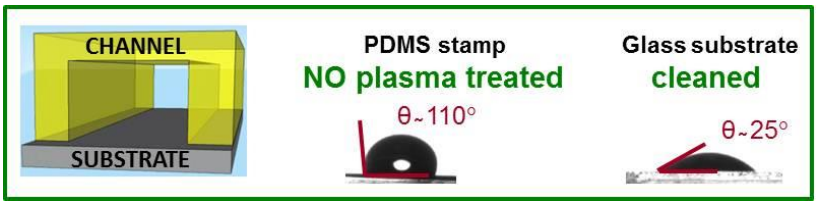

Figure 4.6 Schematic representation of the different PDMS and glass contact angle.

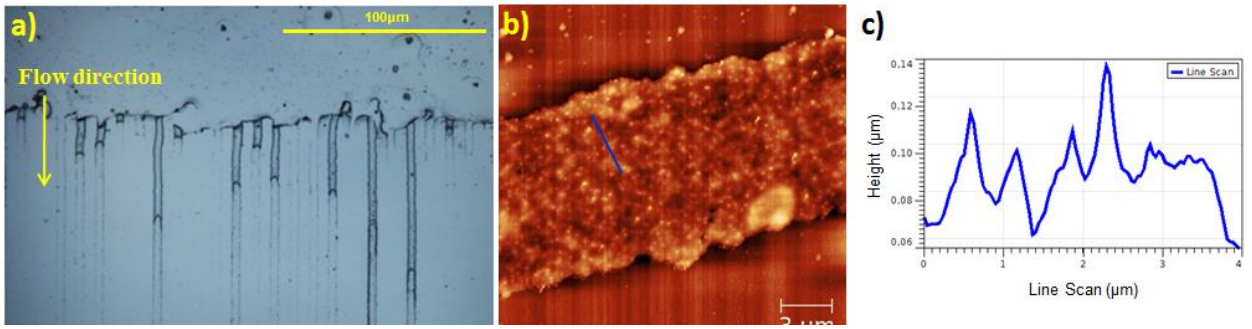

Figure 4.7 (a) Optical micrograph (50X) of ACyD pattern obtained using untreated PDMS stamp; (b) AFM image of the pattern and corresponding line scan (c).

As discussed in Chapter 3, the homogeneous infilling of MIMICs with an aqueous solution requires the modification of the hydrophobic PDMS stamp by means of an air plasma treatment to make the stamp hydrophilic. Since PDMS recovers its hydrophobicity in time, the time between the plasma treatment of PDMS and sealing to the glass substrate has to be matched in such a way that both PDMS and glass have the same contact angle (Figure 4.8). In this manner, the surface tension of the solid-liquid interface is homogeneous inside the channel and we are able to obtain a uniform distribution of ACyD on glass, as we can see from the optical image (Figure 4.9).

Figure 4.8 PDMS stamp and glass substrate will reach about the same contact angle, after the PDMS air plasma surface treatment.

As in the previous case, the stamp was placed onto the glass substrate and a 30 µL droplet solution was deposited on the open end of the stamp and allowed to dry over approximately 2 hours, in air and at room temperature. Then the stamp was gently removed and the sample was scanned by AFM (Figure 4.10). The morphology of the deposit is granular, with a rather broad size dispersion. The profile shows height of the grains on the order of 50-100 nm and full-width-half-maximum (FWHM) of 200-300 nm.

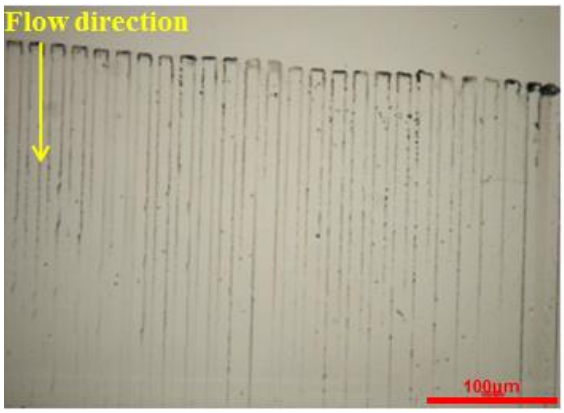

Figure 4.9 Optical micrograph shows the ACyD pattern obtained with MIMICs using a plasma-treated PDMS stamp.

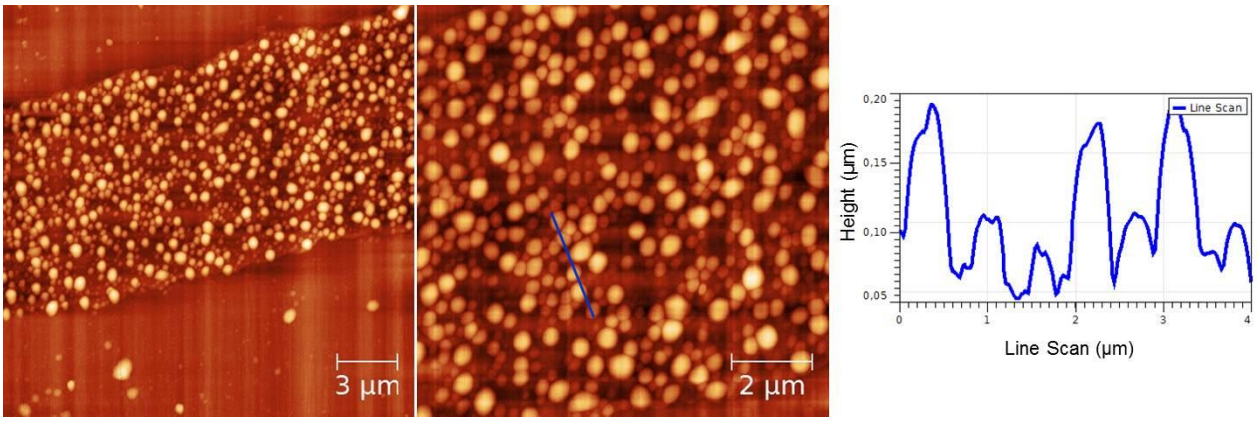

Figure 4.10 AFM images showing the uniform coverage of ACyD on glass and corresponding height profile of the deposits.

4.3 Fabrication of amphiphilic cyclodextrin gradient by microfluidic device

Gradients of chemo-attractant and chemo-repellent substances play central roles in controlling the development of the brain[17]. Although the influence of gradients of soluble substances on neuronal behavior has been extensively studied to unravel the molecular and cellular mechanisms of axon guidance[18], much less is known about cell behavior in the presence of gradients of substrate-bound substances[19]. It would be important to understand the role of immobilized gradients in neuronal development (e.g., establishment of cellular polarity and axon guidance) and cell migration. Generating smooth substrate-bound gradients over the distances relevant to

biological studies (above a few hundred micrometers) is challenging from a technology view point.

By mixing ACyD components bearing different terminal groups and patterning the mixture into a gradient on a surface allows us to obtain accurate cell guidance and localization. The control of the multiscale gradients of chemical cues can be realized by means of a microfluidic device made of PDMS[20]. Networks of micro-channels in PDMS were fabricated by manufacturing the mask with the laser marker then transferring the layout to silicon wafer by photolithography, and finally obtaining PDMS stamp by replica molding.

Our approach to the fabrication of substrate-bound gradients starts from the generation of a solution with ACyD concentration gradient by means of a suitable microfluidic device designed for graded mixing, and the deposition of the proteins in the output solution onto a glass surface. A network with three inlets and nine outlets was used as shown in Figure 4.11.

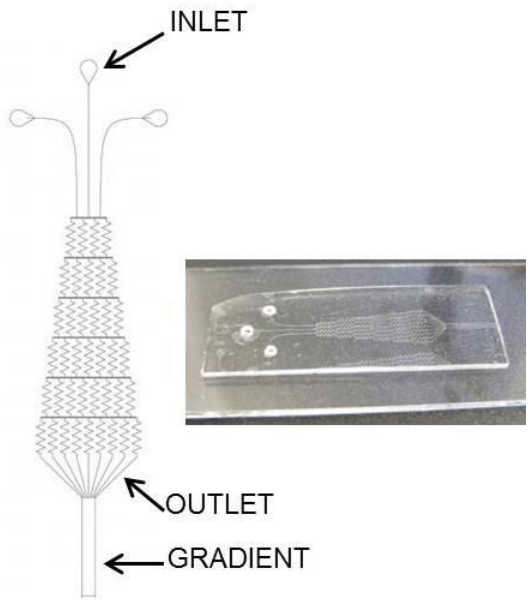

Figure 4.11 Schematic drawing of the design of a typical microfluidic network in PDMS that we used for the fabrication of gradients and real photo of the PDMS stamp on the glass substrate.

The two ACyDs that should be mixed enter at the side inlets, water been injected at the center inlet. At each step, a gradient is generated decreasing in the respective component from the periphery towards the center. At the exit of the microfluidics, the nine outlet channels produce a gradient both longitudinally (in time) and laterally in concentration.

An example that our device works effectively is shown in Figure 4.12. The two test fluids (blue and yellow) are mixed to yield a graded green solution.

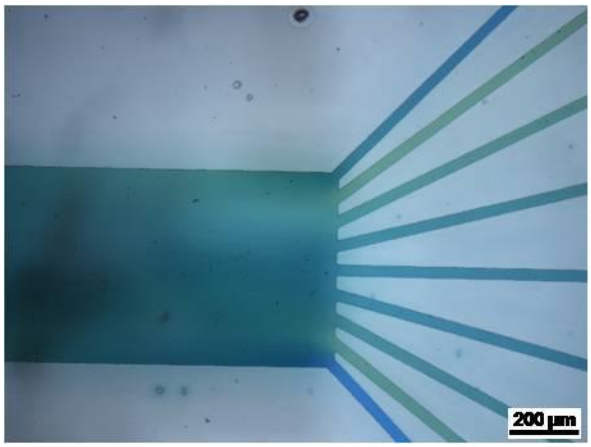

Figure 4.12 Example of gradient obtained by mixing a blue and a yellow inks.

At this stage, the experiments to obtain the mixture of ACyDs is still pending, and the results will not be included in the thesis.

4.4 Conclusions

ACyD have been used as chemical building blocks to be patterned on a surface. It is possible to process them and deposit them as vesicles on a surface either as homogeneous deposit, by MIMICs else in the form of gradient by a microfluidic mixer. Experiments aimed to assess the patterned gradient by means of monitoring the cell behaviour are currently carried out.

Bibliography

[1] H. Honda, M. Tanemura, T. Nagai, *J. Theor. Biol.* **2004**, *226*, 439-453.

[2] a) R. Glass, M. Moller, J. P. Spatz, *Nanotechnology* **2003**, *14*, 1153-1160; b) D. Falconnet, G. Csucs, H. M. Grandin, M. Textor, *Biomaterials* **2006**, *27*, 3044-3063; c) G. Cellot, E. Cilia, S. Cipollone, V. Rancic, A. Sucapane, S. Giordani, L. Gambazzi, H. Markram, M. Grandolfo, D. Scaini, F. Gelain, L. Casalis, M. Prato, M. Giugliano, L. Ballerini, *Nat. Nanotechnol.* **2009**, *4*, 126-133; d) I. Tonazzini, E. Bystrenova, B. Chelli,

P. Greco, P. Stoliar, A. Calo, A. Lazar, F. Borgatti, P. D'Angelo, C. Martini, F. Biscarini, *Biophys. J.* **2010**, *98*, 2804-2812.

[3] T. Reya, S. J. Morrison, M. F. Clarke, I. L. Weissman, *Nature* **2001**, *414*, 105-111.

[4] a) D. E. Discher, P. Janmey, Y. L. Wang, *Science* **2005**, *310*, 1139-1143; b) A. Tampieri, M. Sandri, E. Landi, D. Pressato, S. Francioli, R. Quarto, I. Martin, *Biomaterials* **2008**, *29*, 3539-3546; c) C. Dionigi, M. Bianchi, P. D'Angelo, B. Chelli, P. Greco, A. Shehu, I. Tonazzini, A. N. Lazar, F. Biscarini, *J. Mater. Chem.* **2010**, *20*, 2213-2218; d) F. Valle, B. Chelli, M. Bianchi, P. Greco, E. Bystrenova, I. Tonazzini, F. Biscarini, *Advanced Engineering Materials* **2010**, *12*, B185-B191.

[5] a) M. Cavallini, A. Calo, P. Stoliar, J. C. Kengne, S. Martins, F. C. Matacotta, F. Quist, G. Gbabode, N. Dumont, Y. H. Geerts, F. Biscarini, *Adv. Mater.* **2009**, *21*, 4688-+; b) D. A. Serban, P. Greco, S. Melinte, A. Vlad, C. A. Dutu, S. Zacchini, M. C. Iapalucci, F. Biscarini, M. Cavallini, *Small* **2009**, *5*, 1117-1122.

[6] a) C. Zolkov, D. Avnir, R. Armon, *J. Mater. Chem.* **2004**, *14*, 2200-2205; b) S. S. Jedlicka, J. L. McKenzie, S. J. Leavesley, K. M. Little, T. J. Webster, J. P. Robinson, D. E. Nivens, J. L. Rickus, *J. Mater. Chem.* **2006**, *16*, 3221-3230.

[7] G. Mani, D. M. Johnson, D. Marton, M. D. Feldman, D. Patel, A. A. Ayon, C. M. Agrawal, *Biomaterials* **2008**, *29*, 4561-4573.

[8] a) B. J. Ravoo, R. Darcy, *Angew. Chem., Int. Ed.* **2000**, *39*, 4324-+; b) A. Mazzaglia, R. Donohue, B. J. Ravoo, R. Darcy, *Eur. J. Org. Chem.* **2001**, 1715-1721; c) R. Donohue, A. Mazzaglia, B. J. Ravoo, R. Darcy, *Chem. Commun.* **2002**, 2864-2865.

[9] a) A. Mazzaglia, B. J. Ravoo, R. Darcy, P. Gambadauro, F. Mallamace, *Langmuir* **2002**, *18*, 1945-1948; b) D. Lombardo, A. Longo, R. Darcy, A. Mazzaglia, *Langmuir* **2004**, *20*, 1057-1064.

[10] S. Salmaso, A. Semenzato, P. Caliceti, J. Hoebeke, F. Sonvico, C. Dubernet, P. Couvreur, *Bioconjugate Chem.* **2004**, *15*, 997-1004.

[11] J. Szejtli, *Chem. Rev.* **1998**, *98*, 1743-1753.

[12] W. Saenger, *Angewandte Chemie-International Edition in English* **1980**, *19*, 344-362.

[13] a) K. Uekama, *J. Inclusion Phenom. Macrocyclic Chem.* **2002**, *44*, 3-7; b) T. N. T. Phan, M. Bacquet, M. Morcellet, *React. Funct. Polym.* **2002**, *52*, 117-125; c) A. Harada, *Acc.*

Chem. Res. **2001**, *34*, 456-464; d) S. A. Cryan, R. Donohue, B. J. Ravo, R. Darcy, C. M. O'Driscoll, *Journal of Drug Delivery Science and Technology* **2004**, *14*, 57-62.

[14] A. R. Khan, P. Forgo, K. J. Stine, V. T. D'Souza, *Chem. Rev.* **1998**, *98*, 1977-1996.

[15] K. I. Ogawara, S. Hasegawa, M. Nishikawa, Y. Takakura, M. Hashida, *J. Drug Targeting* **1999**, *6*, 349-360.

[16] J. N. Lee, C. Park, G. M. Whitesides, *Anal. Chem.* **2003**, *75*, 6544-6554.

[17] M. TessierLavigne, C. S. Goodman, *Science* **1996**, *274*, 1123-1133.

[18] H. J. Song, M. M. Poo, *Curr. Opin. Neurobiol.* **1999**, *9*, 355-363.

[19] H. Baier, F. Bonhoeffer, *Science* **1992**, *255*, 472-475.

[20] S. K. W. Dertinger, X. Y. Jiang, Z. Y. Li, V. N. Murthy, G. M. Whitesides, *Proc. Natl. Acad. Sci. U. S. A.* **2002**, *99*, 12542-12547.

[21] D. C. Duffy, J. C. McDonald, O. J. A. Schueller, G. M. Whitesides, *Anal. Chem.* **1998**, *70*, 4974-4984.

CHAPTER 5

Biofunctional scaffold for spinal cord regeneration

In this chapter, fabrication, characterization and functionalization of a biodegradable scaffold that will be integrated with active electronic materials such as organic semiconductors and conductive electrodes, to yield an active multifunctional implantable organic device targeted to the stimulation, monitoring and regeneration of the Spinal Cord Injury are described.

5.1 Introduction

Spinal Cord Injury (SCI) is a damage or trauma to the spinal cord that results in a loss or impaired function causing reduced mobility or feeling. SCI is a devastating and debilitating condition affecting 2.5 million people worldwide, with more than 130000 new cases reported each year. The incidence (average number per million inhabitants per year) estimated is 51 in the Northern America, 19.4 in Europe, 16.8 in Australia and 23.9 in Asia[1]. SCI has a significant impact on quality of life, life expectancy and economic burden, with considerable costs associated with primary care and loss of income. The SCI pathophysiology involves severance of axons, loss of neurons and glia and demyelination associated with a secondary inflammatory degenerative process leading to variable extension of the lesion area and, thus, to different functional deficits. The severity of SCI is adversely correlated with the number of surviving axons at the injury site.

Several experimental regenerative therapies have been developed in the last few years[2]. At present, none of these approaches provides full recovery both in experimental injury models as well as in humans[3]. The recent advances in stem cell biology have raised great expectations that injuries to the spinal cord may be ameliorated by the development and delivery of variably potent stem cells[4]. However, a limited degree of tissue repair and/or protection is achieved in pre-clinical models of SCI, upon focal transplantation of stem cells, including somatic and induced pluripotent stem (iPS) cell-derived neural stem/precursor cells (NPCs)[5]. This is generally attributed to small numbers of transplanted NPCs that survive at the injury site, while progressing towards preferential neuronal[6] or glial[7] differentiation processes, or both[5]. The gold standard cells for tissue regeneration in SCI are expected to survive after transplantation, then to functionally integrate into the host tissue, while differentiating into functional neurons that establish new synapses *in-vivo*. This hypothesis requires either stem cells with remarkable lineage plasticity, as well as well-established safety profile, or implantable multifunctional devices suitable for instructing precise differentiation pathways to endogenous stem/precursors cells. These devices should have long-term stability associated to high biocompatibility and safety, and reduced risk of a host versus graft immune response. Since stem cell commitment is governed by a combination of topo-electro-chemical stimuli, the device must be able to mimic the local microenvironment for stem/precursor cell recruitment and differentiation. This requires the possibility to perform local stimulation with tunable electric fields, together with local delivery of

growth factors, neurotransmitters, and drugs. The integration of highly sensitive transducers in the implanted device would allow monitoring the status of their generating nerve cells and controlling the local auto-immune inflammatory response.

Our research activities in this field is part of a European Project (Project EU NMP-2011-280772) "Implantable Organic Nano-Electronics" (I-ONE). The vision of I-ONE is to realize an Active Multifunctional Implantable organic Device (AMID) targeted to SCI (Figure 5.1). AMID will supply a combination of topo-electrochemical stimuli to the injured region, thus providing the complex microenvironment required for stem cell commitment. AMID will be an complex object of 2 mm length and 1 mm width integrating: biocompatible and/or biodegradable scaffold, organic field effect transistor (OFET) based on nm-thick organic semiconductor, microfluidics and organic electronic ion pumps for local delivery, patterned interfaces, mouse stem cells.

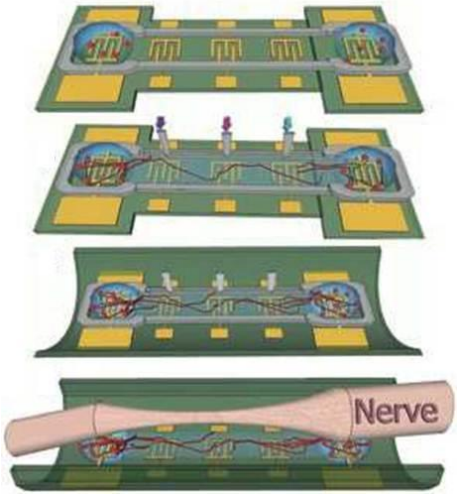

Figure 5.1 Schematic drawing of the AMID prototype.

The prototype AMID devices will be first tested *in-vitro* on regeneration of directed neural network from both mouse somatic spinal cord NPCs and mouse iPS cell-derived NPCs. Both the cell and the organic device responses will be characterized and correlated. The aim is to demonstrate the viability of their construction starting from stem cells. AMID devices will be also tested for their ability to influence the survival and biological activity of immune cells, with the aim of demonstrating the possibility for the AMID device to exert an immune-modulator effect.

AMID is flexible and can be conformally wrapped around the injured nerve or cord (Figure 5.1). It will be engineered into an implantable device whose size is 1-2 mm length x 1 mm diameter. This prototype will be implanted into a contusion mouse SCI animal model. The implantable device life time will be tailored to the time of regeneration. The *in-vivo* demonstration and validation will allow the evaluation of safety and efficacy levels in view of future clinical development.

The level of complexity of the problem targeted by I-ONE requires a converging approach where nanotechnologists, clinical neuroscientists, and high-knowledge content industries are working together. In particular, I was the person in charge to process, characterize and functionalize the scaffold.

5.2 Poly(lactic-co-glycolic)acid as biocompatible and biodegradable scaffold

POLY(LACTIC-CO-GLYCOLIC)ACID (PLGA)

We chose PLGA (Figure 5.2) as scaffold because of the growing interest due to its excellent biocompatibility and biodegradability, as assessed by Food and Drug Administration (FDA) for internal use in human body

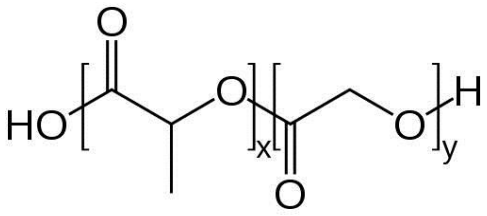

Figure 5.2 Structure of PLGA, where x is the number of lactic acid units and y is number of glycolic acid units.

PLGA is synthesized by means of random ring-opening co-polymerization of two different monomers, the cyclic dimers (1,4-dioxane-2,5-diones) of glycolic acid and lactic acid. The former ends up into the biodegradation path of the oxalic acid, whereas the second enters into the Krebs' cycle. Common catalysts used in the preparation of this polymer include tin(II) 2-ethylhexanoate, tin(II) alkoxides, or aluminum isopropoxide. During polymerization, successive monomeric units of glycolic or lactic acid are linked together in PLGA by ester linkages, thus yielding a linear, aliphatic polyester as a product.

Unlike the homopolymers of lactic acid (polylactide) and glycolic acid (polyglycolide) that show poor solubility, PLGA can be dissolved in a wide range of common solvents, including chlorinated solvents, tetrahydrofuran, acetone or ethyl acetate[8].

The commercially-available PLGA polymers are characterized in terms of intrinsic viscosity, which is directly related to their molecular weights[9]. The mechanical strength, swelling behavior, hydrolysis rate and the related biodegradation are directly influenced by the crystallinity of the PLGA polymer[9]. The resultant crystallinity of the PLGA copolymer is dependent on the type and the molar ratio of the individual monomer components (lactide and glycolide) in the copolymer chain[10]. PLGA polymers containing 50:50 ratio of lactic and glycolic acids are hydrolyzed much faster than those containing higher proportion of either of the two monomers[11]. PLGAs prepared from L-PLA and PGA are crystalline copolymers while those from (D,L)-PLA and PGA are amorphous in nature[9, 11]. Gilding and Reed have pointed out that PLGAs containing less than 70% glycolide are amorphous in nature[12]. The degree of crystallinity and the melting point of the polymers are directly related to the molecular weight of the polymer[9, 11]. The glass transition temperatures (Tg) of PLGA copolymers are above the physiological temperature of 37°C, and hence they are glassy in nature[9, 11]. Jamshidi et al. have reported that Tg of PLGAs decreases with decrease of lactide content in the copolymer composition and with decrease in their molecular weight[13].

Both, *in-vitro* and *in-vivo* the PLGA copolymer undergoes degradation in an aqueous environment (hydrolytic degradation or biodegradation) through cleavage of its backbone ester linkages[9-11, 14]. The polymer chains undergo bulk degradation that occurs at uniform rate throughout the PLGA matrix[9, 14b]. The number of carboxylic end groups present in the PLGA chains increase during the biodegradation process as the individual polymer chains are cleaved; these are known to catalyze the biodegradation process[9, 11]. The biodegradation rate of the PLGA copolymers depend on the molar ratio of the lactic and glycolic acids in the polymer chain, molecular weight of the polymer, the degree of crystallinity, and the Tg of the polymer[9, 11, 14b].

A three-phase mechanism for the PLGA biodegradation has been proposed[15]:

- random chain scission process. The molecular weight of the polymer decreases significantly, but no appreciable weight loss and no soluble monomer products formed;

- in the middle phase a decrease in molecular weight accompanied by rapid loss of mass and soluble oligomeric and monomer products are formed;
- complete polymer solubilization: monomer products formed from soluble oligomeric fragments.

The role of enzymes in any PLGA biodegradation is unclear[9]. Most of the literature indicates that the PLGA biodegradation does not involve any enzymatic activity and is purely through hydrolysis[9]. Some investigators have suggested enzymatic role in PLGA breakdown based upon the difference in the *in-vitro* and *in-vivo* degradation rates[11]. The PLGA polymer biodegrades into lactic and glycolic acids[9-11, 14]. Lactic acid enters the tricarboxylic acid cycle and is metabolized and subsequently eliminated from the body as carbon dioxide and water[9-11, 16]. Glycolic acid is either excreted unchanged in the kidney or enters the tricarboxylic acid cycle and is eventually eliminated as carbondioxide and water[9]. Since the body effectively deals with the two monomers, there is minimal systemic toxicity associated with using PLGA for drug delivery or biomaterial applications.

FABRICATION OF PLGA FILMBY SOLVENT CASTING

PLGA (molecular weight: 66000 - 107000) which is composed by a 75:25 ratio of D,L-lactide and glycolide units, was purchased from Sigma-Aldrich (P1941) and used as received.

PLGA film was prepared by solution casting method[17]. It was dissolved in chloroform under stirring, for about 40 minutes at room temperature, to obtain a 5% wt solution. 100µL of this solution was then cast onto a cleaned glass slide (Thermo Scientific) into a square frame (Sigma, S1815, SecureSlip™ glass coverslip, silicon, 1.2cm x 1.2cm) so as to obtain a thin layer of the solution with a defined geometry and thickness. The solvent was allowed to evaporate at 37°C in an oven for 5 hours, then the frame was removed (Figure 5.3). The resulting transparent film was then disinfected in 99% ethanol for 15 minutes and dried in air before using it. PLGA films were left on the glass substrate for the duration of all experiments.

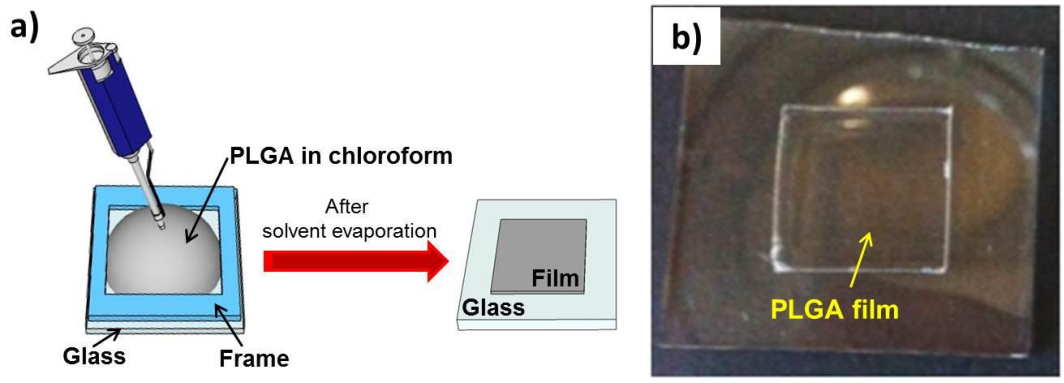

Figure 5.3 (a) Schematic drawing of the solvent casting method used in our experiments; (b) photo of the PLGA film on the glass substrate after the solvent evaporation process.

During the film preparation we realized that the solvent evaporation method was very important. If the solvent was allowed to evaporate in air at room temperature, we did not obtain transparent films each time. This happens because the scarce control the relative humidity of the environment is accompanied by the occurrence of dewetting and breath figures (Figure 5.4). Instead, if the solvent was allowed to evaporate at 37°C in an oven, with a constant relative humidity of 30%, we achieved transparent and uniform film all the time (Figure 5.3b).

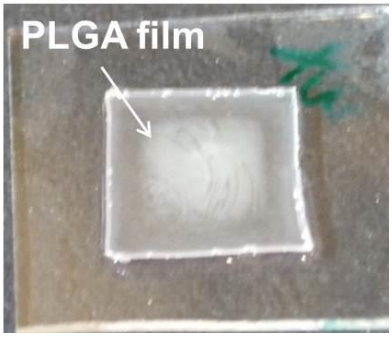

Figure 5.4 Photo a PLGA film obtained sometimes after the solvent evaporation process in air and at room temperature (uncontrolled).

PLGA FILM CHARACTERIZATION

PLGA films were characterized by i) optical microscope; ii) AFM to examine the surface topography; iii) water contact angle to assess the hydrophobicity and iv) optical profilometer to evaluate the thickness.

i) The structure of the films fabricated was observed under a Nikon 80i optical microscope at a magnification of 50X (Figure 5.5).

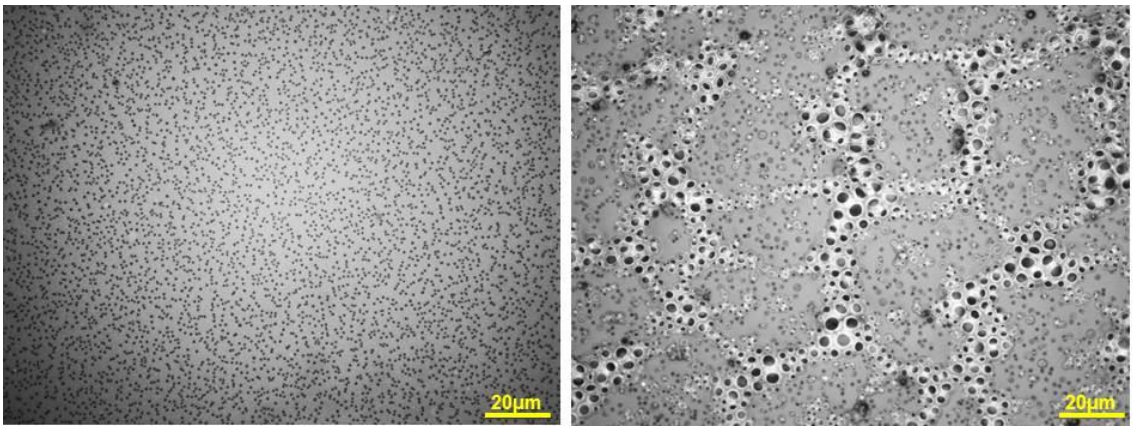

Figure 5.5 Optical micrograph of a PLGA film after solvent evaporation in oven at 37°C (on the left) or in air (on the right).

As from Figure 5.5 the morphology of the film prepared at 37°C is more homogeneous with respect to the one observed in the case of solvent evaporation under ambient conditions.

ii) PLGA films were analyzed by AFM before and after disinfection in ethanol (Figure 5.6). All data were acquired in air using a SMENA NT-MDT scanning probe microscope operated in tapping mode and using silicon cantilever. We observed that the surface of the films were very smooth, with a RMS roughness of about 2 nm in the area without holes. This information is important in view of the deposition of the organic semiconductor on the PLGA substrates in order to create the organic electronic device.

iii) Air/water contact angles were measured with a contact angle goniometer (DGD-DX model, DIGIDROP) and drop shape analysis software of the instrument using the captured drop method on PLGA films before and after the treatment with ethanol at room temperature. Values obtained represent the average ands tandard deviation of three measurements taken from each of five samples for a total of 15 measurements. We noticed that after the solvent evaporation, films were hydrophobic and they had a contact angle of 88°±2°; while after the disinfection process, the films remain hydrophobic, but the contact angle became 79°±1°.

iv) Optical profilometer was used to determine the thickness of the PLGA film. This is a rapid, nondestructive, and noncontact surface metrology technique. An optical profiler is a type of microscope in which light from a lamp is split into two paths by a beam splitter. One path directs

the light onto the surface under test, the other path directs the light to a reference mirror. Reflections from the two interfaces are recombined and projected onto an array detector. When the path difference between the recombined beams is the order of a few wavelengths of light or less interference can occur. This interference contains information about the surface contours of the test surface. Vertical resolution can be the order of several angstroms while lateral resolution depends upon the objective and is typically in the range of 0.5-5 microns. With this technique it is possible to evaluate some typical characteristics of a sample, such as its surface topography, coating thickness and step height.

Experimentally, we measured the thickness of the film on the borders and in the middle and we noticed that the film has a thickness of about 20 µm.

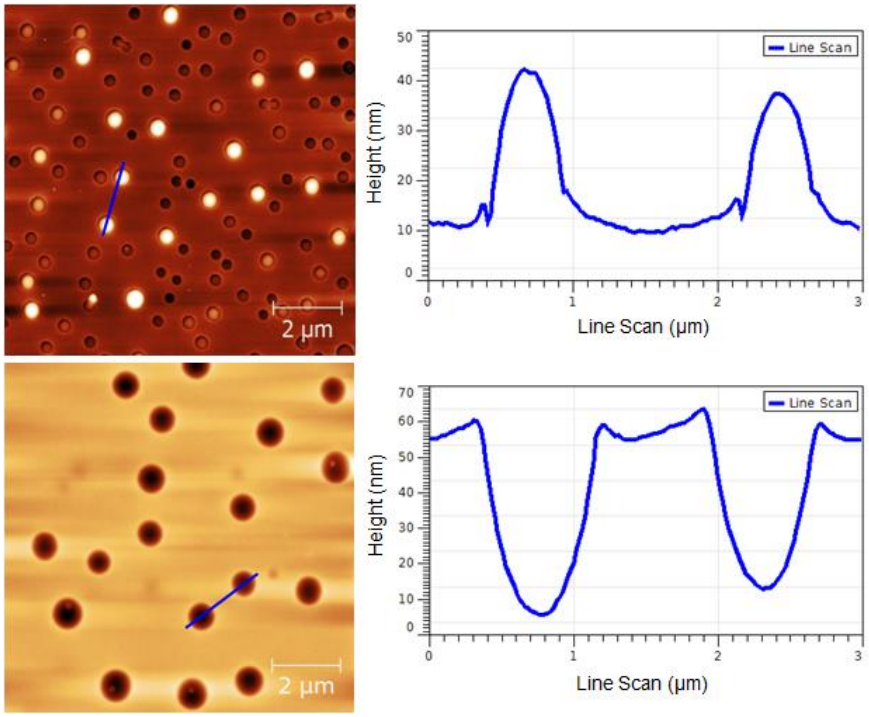

Figure 5.6 Typical AFM images (10x10 µm) and corresponding line scans of a PLGA film obtained after the solvent evaporation (top) and after the disinfection in ethanol (below).

5.3 Laminin functionalization of poly(lactic-co-glycolic)acid films

INTRODUCTION

Precisely controlling cell positioning and growth on a surface is crucial in the field of biosensors[18], medical diagnostics[19], bioelectronics[20] and tissue-engineering[21]. Especially the

recruiting and growth of NPCs are of great potential in the therapy of spinal cord injuries[22] and neurodegenerative diseases of the central nervous system[23].

Although the PLGA film has been investigated in neural tissue-engineering applications because of its tunable mechanical strength and desirable biodegradability, its hydrophobic property gives rise to the poor cell affinity on the surface and limits its application. In order to increase cell adhesion and proliferation on PLGA surface, one can make it more hydrophilic else can deposit a material with fouling properties.

There have been few reports[24] on the surface morphology of PLGA after plasma treatment and effect of surface morphology on cell adhesion. Wan et al., showed that the contact angles of the oxygen plasma treated samples decreased from 78° to 45° after 2 min of exposure. When the sample underwent a treatment longer than 10 min, the water contact angles became less than 10°. Although the biocompatibility of PLGA increases, the roughness of the PLGA surface also increases from nano- to micrometer-scale. In our case the requirement for the deposition of a smooth film for electronic device applications makes the ideal surface much smoother than this. For this reason, we decided to pursue the second strategy, and in particular, the use of an adhesion protein, laminin, in order to increase the biocompatibility of the PLGA films.

Laminin (Figure 5.7) is the principal non-collagenic component and biologically active part of the basal lamina, a protein network foundation for most cells an organs[13]. Laminin is a trimeric protein that contains an α-chain, a β-chain, and a γ-chain, found in five, three, and three genetic variants, respectively. The trimeric proteins form a plus sign with one long arm, giving a structure that can bind to other cell membrane and extracellular matrix molecules. The three shorter arms are able to bind to other laminin molecules, allowing them to form sheets. The long arm is capable of binding to cells, which helps anchor organized tissue cells to the membrane.

We demonstrate here that it is possible to achieve a functionalization of PLGA surface with laminin, by exploiting two independent techniques of deposition: incubation and MIMICs. In the first case, the laminin solution is placed on top of the film and after the incubation time it is removed. In the second case, the modulation of the PDMS stamp hydrophobicity providing the formation of a good and uniform pattern of the laminin solution on the film. Valle et al.[25] demonstrated that the cell adhesion on laminin patterned substrates is highly selective, and cell confluence can be achieved exclusively on the laminin patterned regions.

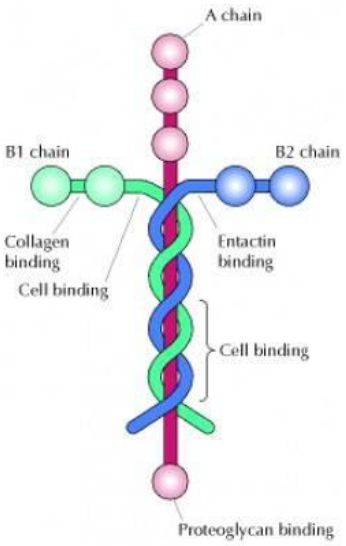

Figure 5.7 Schematic representation of laminin protein, evidencing the trimeric structure.

LAMININ FUNCTIONALIZATION BY INCUBATION

PLGA films have been have been functionalized with laminin by means ofan incubation technique. 150 μL of the laminin solution (5 μg/mL in bi-distilled water) were cast onto the PLGA film. The solution was incubated for 2 hours at room temperature and water was not allowed to evaporate. After the incubation time, the portion of liquid, that was remained on the film, was removed and the film was washed, with PBS 1X and water, in order to take out the excess of laminin on the surface.

Using this functionalization method we are not able to control the distribution of laminin on the PLGA surface and we obtained a non-homogeneous distribution of the protein.

PLGA films with laminin incubated were also characterized by AFM (Figure 5.8). We measured the water contact angle of this substrate and we obtain a value of 78°±1°. We can conclude that the hydrophobicity did not change so much with respect of the cases without laminin.

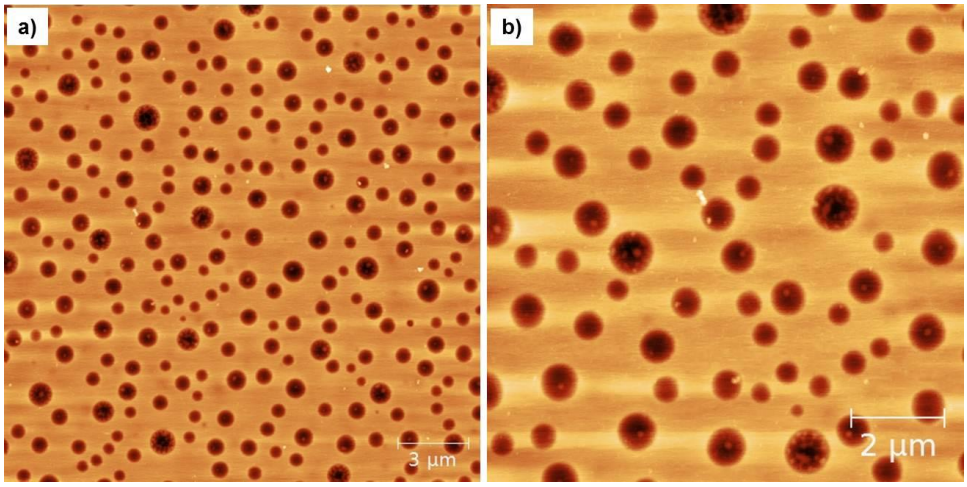

Figure 5.8 (a) 20x20 µm^2 and (b) 10x10 µm^2 AFM images of the PLGA film with laminin incubated for two hours under ambient conditions.

LAMININ FUNCTIONALIZATION BY MIMIC

The functionalization of PLGA films with laminin was then realized by means of MIMICs. The PDMS mold is placed on top of the film and a droplet of 10 µL of laminin solution is placed at the open end of the stamp. The solution is left to evaporate and the stamp is then gently peeled-off. The final pattern of laminin faith fully reproduces the channels of the PDMS stamp.

The PDMS stamp used consists of an array of parallel channels whose width and height are 10µm and 3µm, respectively, and the inter channel distance is 25 µm. Areas as large as 10x7 mm^2 are patterned. The laminin pattern would not be possibly achieved using two extremely hydrophobic surfaces as PDMS and PLGA, because of low Laplace pressure. For this reason we carried out an air plasma treatment of the bottom of the stamp. The bare PDMS surface has a contact angle with pure water of approximately 105°; upon the plasma treatment for 1 minute, the result is 10°, at longer time, it displays a very high hydrophilicity that is more favorable for the laminin solution infilling. Compared to the PDMS stamps plasma treated for 1 minute, the one treated for 15 minutes lead to well uniform stripes over all the patterned area (Figure 5.9).

Figure 5.10 shows an AFM image and the respective height profile of the laminin pattern on PLGA film realized by MIMICs using a PDMS air plasma treated for 15 minutes.

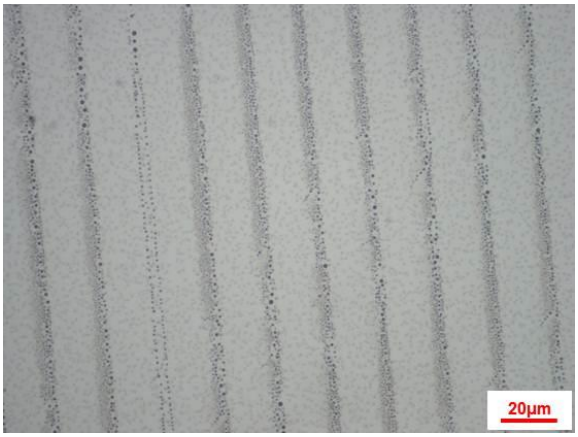

Figure 5.9 Optical micrograph (50X) in bright field showing the laminin pattern (dark stripes) on PLGA surface.

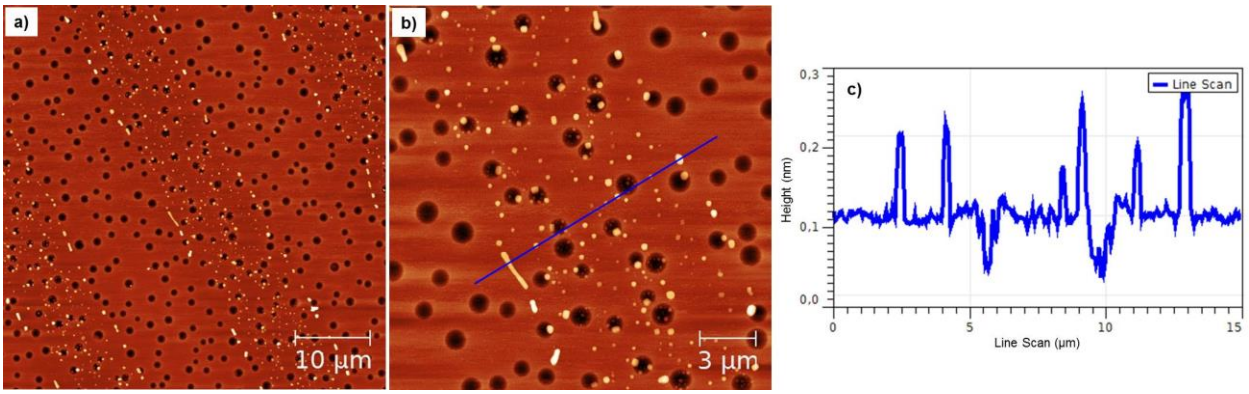

Figure 5.10 (a) and (b) are respectively 50x50 $\mu m^2$and 20x20 μm^2 AFM images of laminin pattern obtained by MIMICs; the line profile in (c) shows the characteristic features of the laminin droplets patterned within the channel.

LAMININ IMMUNOFLUORESCE ASSAY

The distribution of laminin on the substrate and the specific functional binding of the patterned protein have been evaluated also by immunofluorescence assay.

This technique uses the specificity of antibodies to their antigen to tag specific biomolecular targets within a cell with fluorescent dyes, thus allowing visualization of the distribution of the target molecule through the sample. Immunofluorescence is a widely used example of immune staining and is a specific example of immunohistochemistry that makes use of fluorophores to visualize the location of the antibodies.

Laminin patterned PLGA samples were blocked for 1 hour with phosphate buffer saline (PBS) solution 1X containing 1% bovine serum albumin (blocking solution). They were incubated

overnight at 4°C with anti-laminin antibody (L9393 Sigma-Aldrich) diluted 1:50 in blocking solution. Then they were washed three times with a wash buffer (PBS 1X containing 0.05% tween20), and incubated for 90min at room temperature with the fluorescent Alexa Fluor 584 anti-rabbit antibody (Invitrogen) diluted 1:100 in PBS 1X. Control samples were incubated in blocking solution with no primary antibody. After washing with PBS 1X and water, all samples were analyzed under an epifluorescence microscopy (Nikon 80i).

Some experiments were carried out on laminin patterned PLGA substrates, previously maintained in the presence of cell culture medium in standard culture conditions (37 °C in a humidified atmosphere with 5% CO_2) for 6 days.

In Figure 5.11a is shown an optical image of a laminin pattern realized starting from a PDMS stamp with channels of 10 μm and its relative immunofluorescence staining with anti-laminin (Figure 5.11b) also upon incubation for 6 days under the conditions used for cell culture (Figure 5.11c).

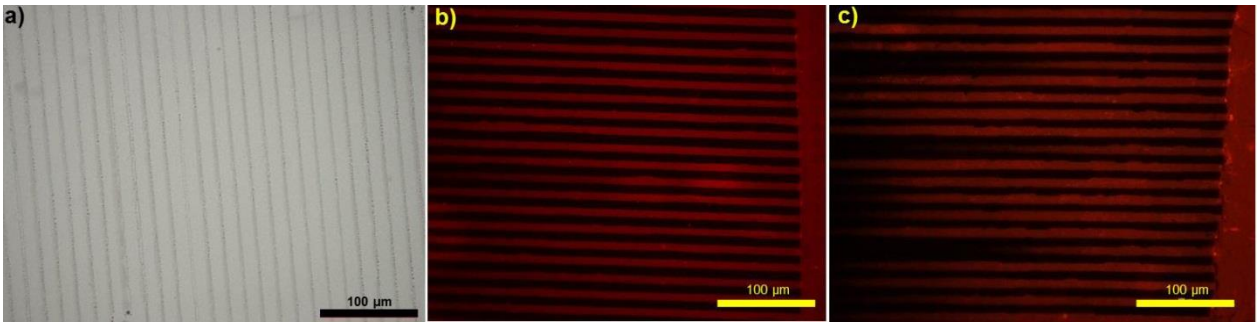

Figure 5.11 (a) Optical image (bright field) of a pattern of laminin with channel 10 μm and its relative immunofluorescence staining with anti-laminin (b) and (c) upon incubation for 6 days under the conditions used for cell culture.

Figure 5.11b clearly shows how the proteins are located along the channels and display their specific binding during incubation time intervals compatible with the cell adhesion and proliferation events. It is worth to stress that the spatially controlled interaction between the laminin and its specific antibody demonstrates how this substrate could be employed for biosensors to detect protein-protein interactions. Remarkably, such a stable controlled functionalization of the substrate has been achieved without any chemical modification of the PLGA substrate by one-step procedure.

5.4 Neural cells growth on poly(lactic-co-glycolic)acid films

To assay the biocompatibility of PLGA films, we tested the ability of spinal cord derived NPCs cells to adhere, survive and differentiate when plated on PLGA. This part of the work was carried out in collaboration with the group of Dr. S. Pluchino in Cambridge, Brain Research Center.

The first trial led to unsatisfactory results due to the poor adhesion of NPCs on the bare PLGA substrates (Figure 5.12a,c), but following experiments resulted in much more convincing data. This was mainly due to a change we made in the coating of the substrate with laminin, which greatly improved the quality of cell adhesion (Figure 5.12b,d). Two different seeding densities (150000 and 200.000 cells/cm^2) were tested and the viability, proliferation and differentiation ability were analyzed at different incubation times (2, 4 and 6 days).

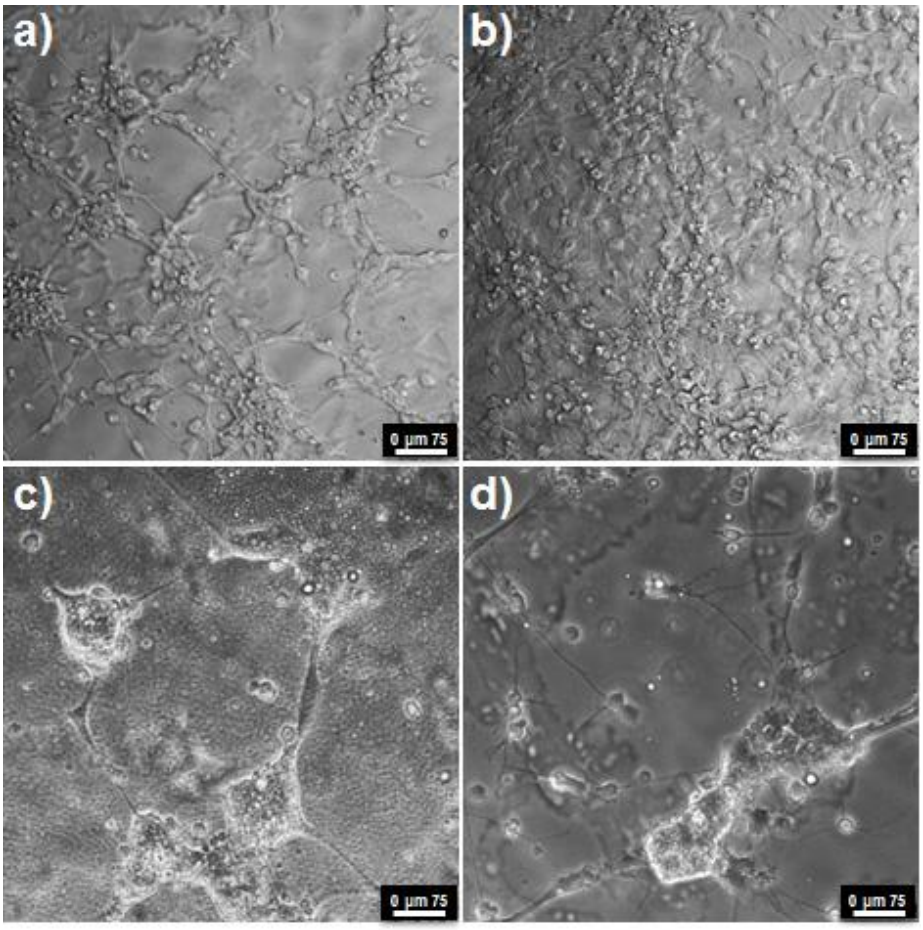

Figure 5.12 (a) Optical image (20X) of NPCs cells on bare PLGA after 24 hours of incubation and (c) after 6 days of incubation in cells culture medium; in (b) and (d) we have the same incubation time of (a) and (c) respectively, but the PLGA was coated with laminin.

Moreover, optical (Figure 5.13a), immunofluorescence (Figure 5.13b), SEM (Figure 5.13c) and AFM (Figure 5.13d) images were acquired on samples integrated with differentiated NPCs evidencing the good adhesion of the cells on PLGA surface and the film integrity.

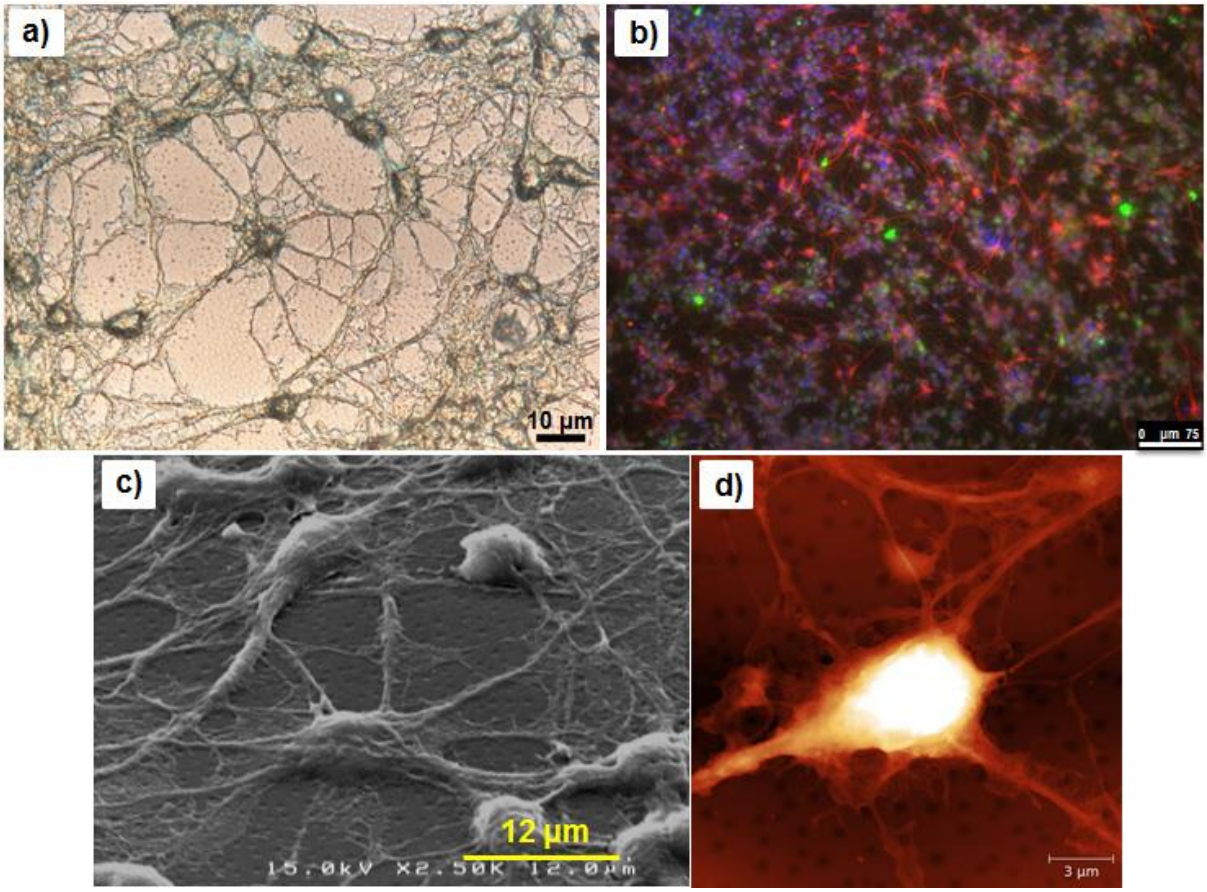

Figure 5.13 (a) Optical, (b) immunofluorescence, (c) SEM and (d) AFM images of NPCs seeded ($2x10^5$ cells/cm^2) on PLGA film pre-coated with laminin after 2 days of incubation.

It is important to underline that SEM analysis requires a specific protocol for the cells fixation. Cells were pre-fixed with glutaraldehyde (2.5% in PBS 1X) for 1 hour at 4°C, washed three times in PBS 1X for 5 minutes at 4°C and one times in water for 5 minutes at room temperature. Then they were post-fixed with osmium tetroxide (1% in distilled water) for 1h at room temperature, washed three times in water for 5 minutes at room temperature and dehydrated in an increasing series of ethanol solution (50%, 75%, 95% and 99%) for 10 minutes each. Subsequently, a thin gold film coating (10 nm) was sputtered before analysis.

The same experiment using PLGA films patterned with laminin is under investigation. To monitor the effectiveness of the functionalization on the control of the cell adhesion and growth, NPC cells will seed on the patterned surfaces and allow to proliferate for 6 days. In Figure 5.14 is reported an immunofluorescence image from the work of Valle et al.[25] that describes this phenomenon. The authors been demonstrated that cells grow only on the laminin pattern while they do not adhere on the outer Teflon-AF surface at all. We would like to achieve the same result also in our study. To date the work is in progress.

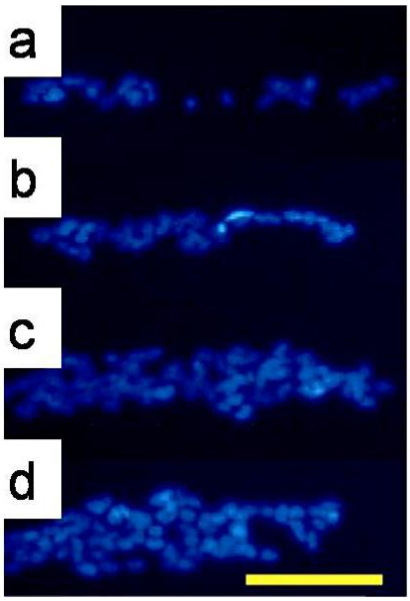

Figure 5.14 (a-d) Neuroblastoma nuclei stained with DAPI (4',6-diamidino-2- phenylindole) attached onto laminin stripes of increasing width[25].

5.5 Conclusions

We have fabricated and fully characterized PLGA film supported on glass. We performed a surface functionalization of this hydrophobic and anti-adhesive substrates by means of incubation and a modified MIMICs patterning which exploits the confinement of the solution of interest between the PLGA surface and the channels of the stamp. Such a confinement has been controlled by the differential wettability of the stamp and the substrate achieved throughout a surface tension modification of the PDMS stamps by air plasma treatment. A non-covalent modification of the surface has been possible without any chemical or physical modification of the PLGA surface thus preserving the relevant properties (such as biocompatibility) of this

material. As a consequence of a well-performed laminin deposition on PLGA, we obtained an extremely selective cell adhesion, both among and along laminin deposits. This approach represents a viable route to the use PLGA-like or other highly hydrophobic materials in tissue engineering as a vector of cells in tissues. The outcome is also a support for the controlled localization and orientation of the cells that is known to play a crucial role in the realization of complex tissues.

Bibliography

[1] M. Wyndaele, J. J. Wyndaele, *Spinal Cord* **2006**, *44*, 523-529.

[2] G. Onose, A. Anghelescu, D. F. Muresanu, L. Padure, M. A. Haras, C. O. Chendreanu, L. V. Onose, A. Mirea, A. V. Ciurea, W. S. El Masri, K. R. H. von Wild, *Spinal Cord* **2009**, *47*, 716-726.

[3] L. Moon, M. B. Bunge, *Journal of neurologic physical therapy : JNPT* **2005**, *29*, 55-69.

[4] O. Lindvall, Z. Kokaia, *J. Clin. Invest.* **2010**, *120*, 29-40.

[5] B. J. Cummings, N. Uchida, S. J. Tamaki, D. L. Salazar, M. Hooshmand, R. Summers, F. H. Gage, A. J. Anderson, *Proc. Natl. Acad. Sci. U. S. A.* **2005**, *102*, 14069-14074.

[6] Y. Ogawa, K. Sawamoto, T. Miyata, S. Miyao, M. Watanabe, M. Nakamura, B. S. Bregman, M. Koike, Y. Uchiyama, Y. Toyama, H. Okano, *J. Neurosci. Res.* **2002**, *69*, 925-933.

[7] S. Karimi-Abdolrezaee, E. Eftekharpour, J. Wang, C. M. Morshead, M. G. Fehlings, *J. Neurosci.* **2006**, *26*, 3377-3389.

[8] a) K. E. Uhrich, S. M. Cannizzaro, R. S. Langer, K. M. Shakesheff, *Chem. Rev.* **1999**, *99*, 3181-3198; b) X. S. Wu, N. Wang, *Journal of Biomaterials Science-Polymer Edition* **2001**, *12*, 21-34.

[9] X. S. Wu, in *Encyclopedic Handbook of Biomaterials and Bioengineering* (Ed.: W. e. al.), Marcel Dekker, New York, **1995**, pp. 1015-1054.

[10] R. Jalil, J. R. Nixon, *J. Microencapsulation* **1990**, *7*, 297-325.

[11] D. H. Lewis, in *Biodegradable polymers as drug delivery systems.* (Ed.: L. R. Chasin M.), Marcel Dekker, New York, **1990**, pp. 1-41.

[12] D. M. Gilding, A. M. Reed, *Polymer* **1979**, *29*, 2229-2234.

[13] K. Jamshidi, S. H. Hyon, Y. Ikada, *Polymer* **1988**, *29*, 2229-2234.

[14] a) J. P. Kitchell, D. L. Wise, *Methods Enzymol.* **1985**, *112*, 436-448; b) S. Cohen, M. J. Alonso, R. Langer, *International journal of technology assessment in health care* **1994**, *10*, 121-130.

[15] R. S. Raghuvanshi, M. Singh, G. P. Talwar, *Int. J. Pharm.* **1993**, *93*, R1-R5.

[16] T. R. Tice, D. R. Cowsar, *Pharm. Technol.* **1984**, *11*, 26-35.

[17] a) T. B. Bini, S. Gao, S. Wang, S. Ramakrishna, *J. Mater. Sci.* **2006**, *41*, 6453-6459; b) J. M. Karp, M. S. Shoichet, J. E. Davies, *Journal of Biomedical Materials Research Part A* **2003**, *64A*, 388-396; c) P. N. Thanki, E. Dellacherie, J.-L. Six, *Appl. Surf. Sci.* **2006**, *253*, 2758-2764.

[18] J. J. Pancrazio, J. P. Whelan, D. A. Borkholder, W. Ma, D. A. Stenger, *Ann. Biomed. Eng.* **1999**, *27*, 697-711.

[19] J. Ziauddin, D. M. Sabatini, *Nature* **2001**, *411*, 107-110.

[20] K. Leong, A. K. Boardman, H. Ma, A. K. Y. Jen, *Langmuir* **2009**, *25*, 4615-4620.

[21] K. B. Lee, S. J. Park, C. A. Mirkin, J. C. Smith, M. Mrksich, *Science* **2002**, *295*, 1702-1705.

[22] Y. D. Teng, E. B. Lavik, X. L. Qu, K. I. Park, J. Ourednik, D. Zurakowski, R. Langer, E. Y. Snyder, *Proc. Natl. Acad. Sci. U. S. A.* **2002**, *99*, 3024-3029.

[23] a) M. B. Bunge, *Neuroscientist* **2001**, *7*, 325-339; b) W. Ma, W. Fitzgerald, Q. Y. Liu, T. J. O'Shaughnessy, D. Maric, H. J. Lin, D. L. Alkon, J. L. Barker, *Exp. Neurol.* **2004**, *190*, 276-288.

[24] a) Y. Wan, X. Qu, J. Lu, C. Zhu, L. Wan, J. Yang, J. Bei, S. Wang, *Biomaterials* **2004**, *25*, 4777-4783; b) N. Hasirci, T. Endogan, E. Vardar, A. Kiziltay, V. Hasirci, *Surf. Interface Anal.* **2010**, *42*, 486-491.

[25] F. Valle, B. Chelli, M. Bianchi, P. Greco, E. Bystrenova, I. Tonazzini, F. Biscarini, *Advanced Engineering Materials* **2010**, *12*, B185-B191.

CONCLUSIONS

I presented different nanotechnology-based approaches for the fabrication of multiscale structures and devices that can be used for studying the behavior of systems relevant to biomedical research. Applications to the study of amyloid peptide aggregation in confined environment, to the spatial and temporal control of the interactions between a biomaterial and cells, and to the fabrication of novel implantable devices aimed to influence cellular behaviour by means of different external stimuli.

The research activity has been focused on microfluidics studies of β-amyloid (Aβ) peptides, and on the patterning of amphiphilic cyclodextrin (ACyD) functionalized with fouling and antifouling cues by MicroMolding in Capillaries.

In the former case, we have studied the early stages of Aβ1-40 peptide aggregation at the solid-liquid interface and how this is influenced by surface tension and confinement. The role of surface tension in affecting the size, the order and the morphology of the final aggregates has been discussed.

Patterns of ACyD onto a glass substrate were used to guide motility, adhesion, functionality and differentiation of cells exposed to topo-chemical stimuli. Our approach takes advantage of a single-step fabrication yielding substrates with micro- and nanometer features. This approach allows us to study the main properties of the biomolecules confined at a scale level comparable to the physiological environment.

Finally, I have fabricated and characterized a poly(lactic-co-glycolic)acid (PLGA) scaffold, which is biocompatible and biodegradable, by means of a solution casting technique. PLGA scaffolds have been used to assess the biocompatibility of the stem cells, namely adhesion and differentiation. As a consequence, this PLGA scaffold will be integrated in an implantable organic device targeted to Spinal Cord Injury. The PLGA scaffold treated with stem cells can satisfy the stringent requirements of such device.

In conclusion, this work highlights the versatility and impact of nanotechnology for the control of biomolecules and/or biomaterials aiming at biomedical applications.

Trainings

- Scuola avanzata di Microscopia a Scansione di Sonda, at CNR-ISMN Bologna, Italy (November – December 2011).
- Scuola introduttiva teorico-pratica di Microscopia a Scansione di Sonda, at CNR-ISMN Bologna, Italy (November - December 2010).
- International School of Liquid Crystal, "Organic Nanomaterials for Electronics and Photonics", Erice, Italy (April 2010).

Participation to meetings and conferences

- "Nanotechnology Control of Self Organized Biomolecules and Biomaterials for Medical Research"

  G. Foschi, E.Bystrenova, F. Valle, B. Chelli, S. Casalini, T.Cramer, M.Barbalinardo, F. Leonardi, A.Campana, P. Greco and F. Biscarini

  Gioranta della Chimica in Emilia Romagna, Ferrara (Italy), December 2012.
- "Multiscale patterning fabrication to study biomolecules in confined environments"

  G. Foschi, E. Bystrenova, F. Valle, B. Chelli, M. Barbalinardo, P. Greco and F. Biscarini

  9th International Conference on Nanosciences & Nanotechnologies (NN12), Thessaloniki, Grece, 3-6 July 2012.
- "Fabrication, characterization and porosity analysis of a scaffold based on a standing fibrin film"

  M. Barbvalinardo, F. Valle, B. Chelli, E. Bystrenova, **G. Foschi** and F.Biscarini

  9th International Conference on Nanosciences & Nanotechnologies (NN12), Thessaloniki, Grece, 3-6 July 2012.

- "Surface tension of microfluidic environments affects the early stage aggregation of β-amyloid peptide"

  G. Foschi, E. Bystrenova, F. Valle, P. Greco and F. Biscarini

  6° Meeting in Nuove Prospettive in Chimica Farmaceutica (NPCF6), Riccione (Italy), April 2012.

- "Multiple length scale pattern fabbrication for regenerative medicine"

  B. Chelli, E. Bystrenova, F. Valle, M. Bianchi, M. Barbalinardo, A. Shehu, T. Cramer, **G. Foschi**, M. Murgia, A. Piccoli, P. Greco and F. Biscarini

  X Convegno Materiali Nanofasici, Bologna (Italy), September 2011.

- "Confinement affects amyloid peptide structure - Atomic Force Microscopy study"

  G. Foschi, E. Bystrenova, P. Greco and F. Biscarini

  10th Multinational Congress on Microscopy 2011, Urbino (Italy), September 2011.

- "Nanotechnology-useful technique for study of Alzheimer's disease"

  G. Foschi, E. Bystrenova, P. Greco and F. Biscarini

  Workshop in honour of Carlo Taliani, Bologna (Italy), May 2011.

- "Confinement makes amyloid peptide oligomers stable"

  G. Foschi, E. Bystrenova, A. N. Lazar, P. Greco and F. Biscarini.

  XIII. Linz Winter School and Workshop, Linz (Austria), February 2011.

- "Multiscale patterning for regenerative medicine."

  E. Bystrenova, F. Valle, B. Chelli, M. Bianchi, P. Greco, A. Bergia, **G. Foschi**, M. Barbalinardo, M., Cavallini and F. Biscarini.

  Turkish Italian Workshop on the Frontiers in Nanomaterial Research and Applications, Istanbul (Turkey), December 2010.

Publications

- "Surface Tension in Confined Environment Affects the Early Stage Aggregation of Amyloid β 1-40 Peptide", **G. Foschi**, E. Bystrenova, F. Valle, C. Albonetti, F. Liscio, P. Greco and F. Biscarini, submitted to *Chem. Phys Chem*., **2012**.

- "Applications of Dewetting in Micro and Nonotechnology"
  D. Gentili, **G. Foschi**, F. Valle, M. Cavallini and F.Biscarini, *Chem. Soc. Rev.*, **2012**, *41*, 4430-4443.
- "Multiscale pattern fabrication for life-science applications"
  F. Valle, B. Chelli, M. Bianchi, E. Bystrenova, M. Barbalinardo, A. Shehu, T. Cramer, M. Murgia, **G. Foschi**, P. Greco, M. Cavallini and F. Biscarini, *European Biophysics Journal with Biophysics Letters*, **2011**, *40*, 233-234.

Ringraziamenti

Mi sembra doveroso iniziare ringraziando il Prof. Fabio Biscarini per tutto ciò che mi ha trasmesso, per la sua disponibilità e per tutto quello che ha fatto per portarmi fino a questo traguardo.

Un ringraziamento particolare va anche ad Eva e Francesco per tutte le cose che mi hanno insegnato e perché hanno sempre saputo trovare parole incoraggianti anche nei momenti più difficili.

Grazie a tutti i ragazzi del laboratorio, Adrica, Alessandra, Beatrice, Crispin, Cristiano (che mi ha soprannominato "faccine"), Mauro, Massimiliano (Max), Patrizia, Silvia, Stefano (Chiodo), Tobias e Zahra, per la loro presenza in ogni momento, per tutte le risate fatte insieme e i bei momenti passati.

Un grazie speciale va riservato a Marianna e Francesca, le due ragazze che durante tutto questo periodo insieme a me hanno fatto parte del "Chicken Corner" e che non mi hanno mai lasciata da sola. Sono davvero molto contenta di aver incontrato due persone speciali come loro.

Grazie a Denis e a Stefano (Casolo) per gli ottimi consigli e per avermi sempre spronato a dare il meglio.

Ovviamente un grazie speciale va a tutta la mia famiglia e in modo particolare, a mia madre Paola, a mio padre Maurizio e alle mie nonne Argentina (Argi) e Bruna, perché hanno sempre sostenuto ogni mi scelta e decisione e perché sanno capirmi e sopportarmi.

Ultimo, ma non per questo meno importante, grazie a Michele, forse l'unico che ha vissuto e che vive quotidianamente ogni momento accanto a me, che mi sopporta anche quando torno a casa stanca e intrattabile, ma soprattutto perché riesce a farmi capire quali sono le cose davvero importanti.

Un grazie a tutti coloro che non ho nominato esplicitamente, me che porto sempre nel mio cuore.

GRAZIE A TUTTI VOI!!!